© 2023. Published by The Company of Biologists Ltd | Development (2023) 150, dev201535. doi:10.1242/dev.201535

RESEARCH ARTICLE

Global SUMOylation in mouse oocytes maintains oocyte identity and regulates chromatin remodeling and transcriptional silencing at the end of folliculogenesis

Shawn M. Briley[1,2], Avery A. Ahmed[2,3], Tessa E. Steenwinkel[2,3], Peixin Jiang[2], Sean M. Hartig[4,5,6], Karen Schindler[7] and Stephanie A. Pangas[1,2,3,6,*]

ABSTRACT

Meiotically competent oocytes in mammals undergo cyclic development during folliculogenesis. Oocytes within ovarian follicles are transcriptionally active, producing and storing transcripts required for oocyte growth, somatic cell communication and early embryogenesis. Transcription ceases as oocytes transition from growth to maturation and does not resume until zygotic genome activation. Although SUMOylation, a post-translational modification, plays multifaceted roles in transcriptional regulation, its involvement during oocyte development remains poorly understood. In this study, we generated an oocyte-specific knockout of *Ube2i*, encoding the SUMO E2 enzyme UBE2I, using *Zp3-cre+* to determine how loss of oocyte SUMOylation during folliculogenesis affects oocyte development. *Ube2i Zp3-cre+* female knockout mice were sterile, with oocyte defects in meiotic competence, spindle architecture and chromosome alignment, and a premature arrest in metaphase I. Additionally, fully grown *Ube2i Zp3-cre+* oocytes exhibited sustained transcriptional activity but downregulated maternal effect genes and prematurely activated genes and retrotransposons typically associated with zygotic genome activation. These findings demonstrate that UBE2I is required for the acquisition of key hallmarks of oocyte development during folliculogenesis, and highlight UBE2I as a previously unreported orchestrator of transcriptional regulation in mouse oocytes.

KEY WORDS: SUMOylation, UBC9, Fertility, Germ cell

INTRODUCTION

In mammals, oocyte development begins embryonically but is not completed until the oocyte is fertilized following ovulation in adults. Prior to birth, mouse oocytes begin meiosis and proceed through the early stages of prophase I to arrest in the diplotene stage (Bullejos and Koopman, 2004; Schindler, 2011). Oocytes remain arrested in prophase I while stored as primordial follicles and following recruitment into the growing pool of follicles, where they develop to fully grown oocytes capable of resuming meiosis, i.e. meiotic competence. During folliculogenesis, prophase I oocytes are transcriptionally active, producing and storing transcripts needed for meiotic maturation and early embryogenesis; once fully grown, oocyte transcription is silenced and the chromatin undergoes structural changes within the nucleus (also called the 'germinal vesicle' or GV) (De La Fuente and Eppig, 2001; Albertini, 2002). Following the luteinizing hormone (LH) surge, oocytes resume meiosis, the nuclear envelope breaks down (GV breakdown or GVBD), and the process of spindle assembly begins and ovulation occurs. Oocytes proceed through pro-metaphase to reach metaphase I (MI) and must satisfy the spindle assembly checkpoint (SAC) before homologous chromosomes are separated and the first polar body is extruded, marking the end of meiosis I. A second meiotic arrest then occurs at metaphase II (MII), where the oocytes, now referred to as eggs, remain arrested until fertilization (Tripathi et al., 2010). Oocytes are transcriptionally silent throughout meiotic maturation and transcription does not resume until after fertilization when zygotic genome activation (ZGA) occurs during the maternal-to-zygotic transition (Lee et al., 2014; Aoki, 2022).

SUMOylation is an essential covalent post-translational modification wherein a small ubiquitin-like modifier protein (SUMO1-4) is attached to a lysine of the target protein at a specific sequence. SUMOylation uses a stepwise enzymatic cascade (E1 'activating', E2 'conjugating' and E3 'ligase' enzymes), similar to ubiquitination. There is only one known E2 enzyme in the SUMOylation pathway, UBE2I (also known as UBC9) and mice lacking *Ube2i* die early post-implantation with defects in chromosome condensation and segregation and a range of nuclear structural defects (Nacerddine et al., 2005). SUMOylation impacts diverse functions, but predominantly targets nuclear proteins and regulates DNA replication, DNA damage repair and chromatin (Neyret-Kahn et al., 2013; Cossec et al., 2018; Garvin, 2019; Theurillat et al., 2020; Abbas, 2021; Vertegaal, 2022). SUMOylation also maintains mouse embryonic stem cell identity and pluripotency (Nacerddine et al., 2005; Cossec et al., 2018; Vertegaal, 2022). Model systems, particularly yeast, have shown SUMOylation as a key regulator of meiosis, chromatin configuration, and transcriptional activity, but the role of SUMOylation during mammalian oocyte development is largely uncharacterized, particularly during the critical growth phase within ovarian follicles when prophase I-arrested oocytes attain meiotic and developmental competence (Buccione et al., 1990; Zhu et al., 2010; Yuan et al., 2014; Nottke et al., 2017; Feitosa et al., 2018; Feitosa and Morris, 2018; Rodriguez et al., 2019; Bhagwat et al., 2021).

[1]Graduate Program in Biochemistry and Molecular Biology, Baylor College of Medicine, Houston, TX 77030, USA. [2]Department of Pathology & Immunology, Baylor College of Medicine, Houston, TX 77030, USA. [3]Graduate Program in Development, Disease Models & Therapeutics, Baylor College of Medicine, Houston, TX 77030, USA. [4]Division of Diabetes, Endocrinology, & Metabolism, Baylor College of Medicine, Houston, TX 77030, USA. [5]Department of Medicine, Baylor College of Medicine, Houston, TX 77030, USA. [6]Department of Molecular & Cellular Biology, Baylor College of Medicine, Houston, TX 77030, USA. [7]Department of Genetics, Rutgers, The State University of New Jersey, Piscataway, NJ 08854, USA.

*Author for correspondence (spangas@bcm.edu)

S.A.P., 0000-0001-5748-5844

Handling Editor: Liz Robertson
Received 14 December 2022; Accepted 31 July 2023

Development (2023) 150, dev201535. doi:10.1242/dev.201535

We previously generated a mouse model with conditional deletion of *Ube2i* in oocytes beginning at the primordial follicle stage (i.e. prior to the start of folliculogenesis) (Rodriguez et al., 2019). Female mice were sterile with premature depletion of both resting and growing ovarian follicles in early adulthood, reminiscent of primary ovarian insufficiency. Loss of both resting (primordial) and growing follicles suggested that oocyte SUMOylation was required for the stability of both populations (Rodriguez et al., 2019), but it was unknown whether loss of primordial follicles was directly due to oocyte defects or an indirect consequence caused by loss of regulatory factors from growing follicles (Durlinger et al., 1999, 2002; Mizunuma et al., 1999; Fortune, 2002). To test this, we generated a *Ube2i* oocyte knockout using *Zp3-cre*+, an oocyte-specific cre recombinase line that deletes *loxP*-flanked ('floxed') alleles only in growing follicles (Lan et al., 2004). Here, we show that *Ube2i Zp3-cre*+ female mice are sterile but have a stable ovarian reserve. Phenotype analysis of *Ube2i Zp3cre*+ mice uncovered additional roles for UBE2I in mouse oocytes that include establishing a fully condensed chromatin configuration, regulating global transcriptional silencing and preventing premature activation of genes typically associated with ZGA. Thus, our approach uncovered SUMOylation as a major regulatory process for key events in mouse oocyte development, which must be established by the end of folliculogenesis.

RESULTS

Oocyte-specific deletion of *Ube2i* at the primary follicle stage causes female sterility but maintains the ovarian reserve

To determine the role of UBE2I in growing oocytes, male mice carrying cre recombinase under control of regulatory sequences of the mouse zona pellucida 3 (*Zp3*) gene (*Zp3-cre*) were crossed to $Ube2i^{loxP/loxP}$ female mice (Cox et al., 2021) to delete *Ube2i* in oocytes within growing primary follicles (Fig. 1A). This conditional allele of *Ube2i* deletes exons 3 and 4, whereas our prior conditional knockout model deletes *Ube2i* exons 2 and 3 (Rodriguez et al., 2019); both *Ube2i* conditional alleles generate null alleles following recombination (Rodriguez et al., 2019; Cox et al., 2021). We validated that the conditional deletion of $Ube2i^{loxP/loxP}$ (Δ3-4) using *Gdf9-icre*+ generates a similar phenotype to $Ube2i^{loxP/loxP}$ *Gdf9-icre*+ (Δ2-3) (Rodriguez et al., 2019) by testing fertility over 6 months and assessing ovarian histology. Both the new $Ube2i^{loxP/loxP}$ (Δ3-4) *Gdf9-icre*+ and the published $Ube2i^{loxP/loxP}$ *Gdf9-icre*+ (Δ2-3) were female sterile, with full depletion of ovarian follicles by 6 months of age (Fig. S1). The studies herein used the $Ube2i^{loxP/loxP}$ (Δ3-4) allele for conditional deletion.

$Ube2i^{loxP/loxP}$ *Zp3-cre*+ oocytes (termed '*Ube2i Zp3-cre*+') were validated for loss of *Ube2i* using quantitative reverse transcription PCR (RT-qPCR) and indirect immunofluorescence. By RT-qPCR, fully grown, prophase I-arrested GV oocytes isolated from *Ube2i Zp3-cre*+ antral follicles showed a 99.4% reduction in *Ube2i* transcripts compared with transcript levels in control ($Ube2i^{loxP/loxP}$) littermates ($P<0.0001$) (Fig. 1B). Indirect immunofluorescence of UBE2I demonstrated loss of the UBE2I protein specifically in oocytes of growing follicles but not in oocytes in primordial follicles in *Ube2i Zp3-cre*+ mice (Fig. S2). Specificity of oocyte deletion was verified by RT-qPCR of *Ube2i* in granulosa cells and the presence of UBE2I protein in cumulus cells between genotypes (Figs S2 and S3). To determine whether loss of *Ube2i* in oocytes of growing follicles affected fertility, 6-week-old control or *Ube2i Zp3-cre*+ female littermates were pair-housed and continually mated with sexually mature wild-type males for 6 months. Although control females produced an average (±s.e.m.) of 6.4±0.5 pups per litter, *Ube2i Zp3-cre*+ females failed to produce any litters, demonstrating that oocyte-specific deletion of *Ube2i* using *Zp3-cre*+ causes female sterility (Fig. 1C, $P=0.0003$).

As both *Ube2i Gdf9-icre*+ models (*Ube2i* Δ3-4 and the published *Ube2i* Δ2-3) show complete depletion of all ovarian follicles by 6 months of age (Fig. S1) (Rodriguez et al., 2019), we assessed whether loss of *Ube2i* in oocytes of growing follicles using *Zp3-cre*+ also affected stability of the ovarian reserve. Ovaries from 6-month-old control and *Ube2i Zp3-cre*+ females were collected, and histology and ovarian follicle morphometrics determined. Unlike 6-month-old *Ube2i Gdf9-icre*+ ovaries (Rodriguez et al., 2019) (Fig. S1), 6-month-old *Ube2i Zp3-cre*+ ovaries were a similar size as that of control ovaries and contained similar follicle stages, including corpora lutea, indicating that ovulation had occurred (Fig. S4). Although ovarian histology was grossly similar between genotypes, some defects were noted in cumulus cells surrounding mutant oocytes. Although it was compact, the cumulus cell layer around oocytes of antral follicles showed fewer layers in *Ube2i Zp3-cre*+ ovaries (Fig. S4E,F). A linear regression analysis of cumulus cell width and antral follicle diameter showed that *Ube2i Gdf9-icre*+ cumulus cells maintained the positive correlation with follicle diameter similar to that of controls, but had an altered growth pattern (Fig. S5). By morphometric analysis, *Ube2i Zp3-cre*+ ovaries contained similar numbers of all follicle stages compared with those for control littermates, except for a small but significant decrease in the number of primary follicles (Fig. S4G). In line with maintenance of the ovarian reserve, *Ube2i Zp3-cre*+ female mice had similar steady state levels of estradiol and follicle-stimulating hormone (FSH) as those of their littermate controls (Fig. 1D,E). Taken together, these results indicate that although loss of *Ube2i* in growing oocytes caused sterility, it minimally disrupted folliculogenesis or ovarian hormonal feedback.

Ube2i Zp3-cre+ oocytes arrest at MI

The presence of corpora lutea in histological sections of ovaries of *Ube2i Zp3-cre*+ mice (Fig. S4B,D) suggest that these mice ovulate despite being sterile. Therefore, we assessed the ability of mice to ovulate using stimulation by exogenous gonadotropin injection ('superovulation'). *Ube2i Zp3-cre*+ females ovulated significantly fewer oocytes/eggs ($P=0.0138$) compared with control females (Fig. 1F). As expected, within the ampulla of the oviduct, eggs from control females were enclosed in an expanded cumulus-oocyte-complex. However, those ovulated from *Ube2i Zp3-cre*+ females had fewer layers of expanded cumulus cells (Fig. S6). In addition, control mice ovulated MII-stage eggs with visible polar bodies as expected; however, ovulated oocytes from *Ube2i Zp3-cre*+ females lacked a visible polar body (Fig. 1G-I). To verify the meiotic stage of the ovulated oocytes, we analyzed for the presence of a spindle via α-tubulin immunostaining and DNA labeling. Control ovulated eggs contained a well-organized MII spindle with chromosome alignment, whereas *Ube2i Zp3-cre*+ oocytes had disorganized spindles, misaligned chromosomes and no polar body, thus appearing to arrest in MI (Fig. 1J,K).

We then determined the ability of fully grown, prophase I-arrested GV oocytes to undergo meiotic resumption and progression *in vitro*. Fully grown, prophase I-arrested GV oocytes were harvested from control and *Ube2i Zp3-cre*+ ovaries following hormone stimulation into medium containing 2.5 µM milrinone, which maintains meiotic arrest, and any remaining cumulus cells were manually removed. Oocytes were collected, washed to remove the milrinone, then cultured for 8.5 h, fixed and analyzed for GVBD

Development (2023) 150, dev201535. doi:10.1242/dev.201535

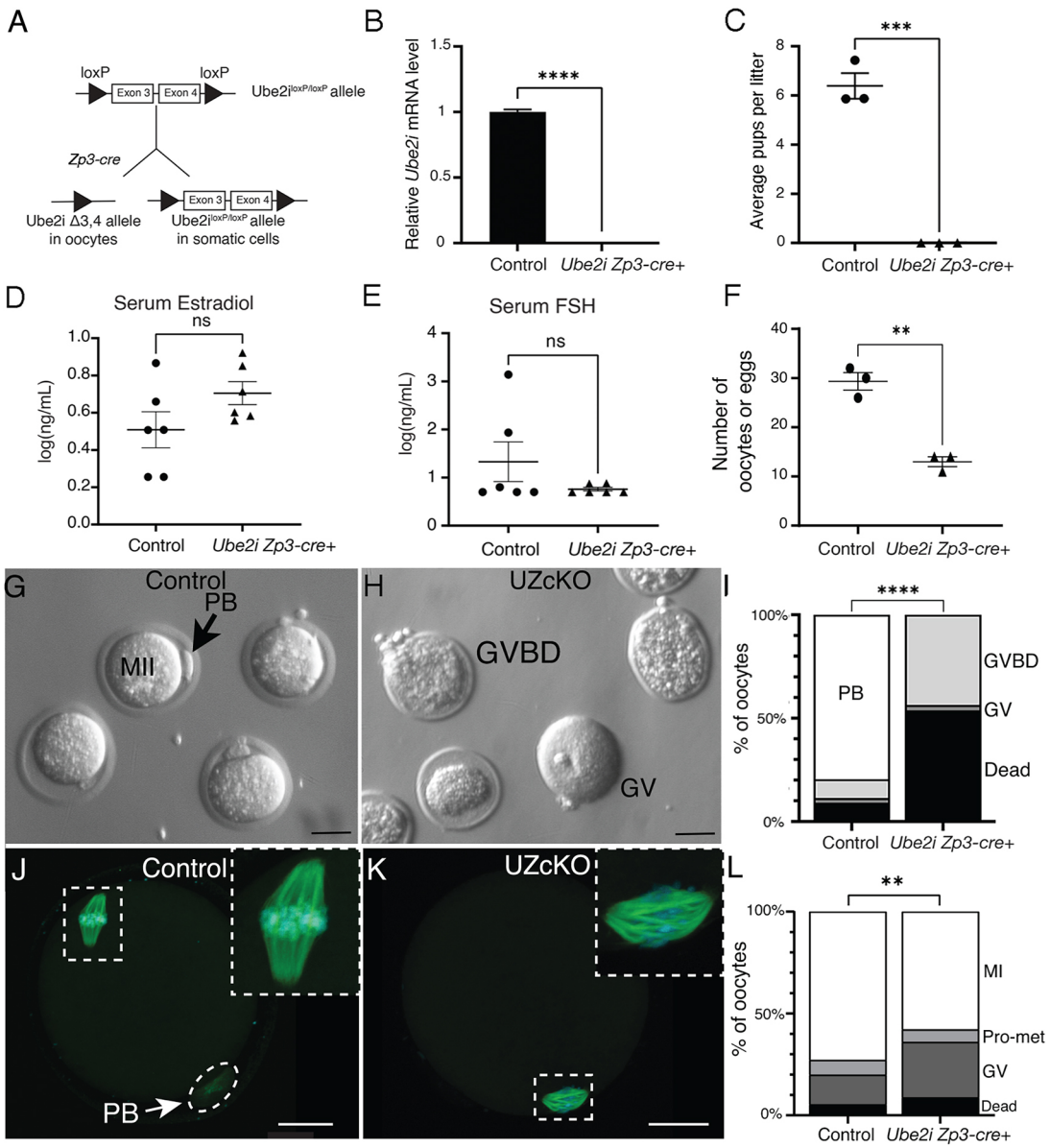

Fig. 1. *Ube2i Zp3-cre+* is female sterile. (A) Schematic for generating *Ube2i Zp3-cre+* mice. (B) RT-qPCR analysis for *Ube2i* expression in fully grown GV oocytes (three pools of *n*=86 *Ube2i Zp3-cre+* or 97 control oocytes) collected from three animals per genotype), normalized to *Ubc* expression and relative to control *Ube2i* mRNA levels, shows depletion of *Ube2i* (****P<0.0001 by unpaired two-tailed *t*-test) with mean±s.e.m. shown. (C) Fertility analysis of control and *Ube2i Zp3-cre+* females (***P=0.0003 by unpaired two-tailed *t*-test, *n*=3 for both genotypes). (D,E) Serum levels of estradiol (D) and FSH (E) between genotypes (*n*=6 per genotype) as measured by ELISA (estradiol, P=0.1171 by unpaired two-tailed *t*-test; FSH, P=0.2269 by Welch's unpaired two-tailed *t*-test; statistical analysis on log-transformed data). (F) Quantification of ovulated oocytes in control and *Ube2i Zp3-cre+* females (**P<0.05 by unpaired two-tailed *t*-test, *n*=3 mice per genotype). (G) Representative images of eggs ovulated from control mice showing a polar body (PB), indicating arrested at MII. (H) Representative images of oocytes ovulated from *Ube2i Zp3-cre+* ('UZ cKO') females lacking PBs. (I) Quantification of meiotic stage of oocytes collected from *Ube2i Zp3-cre+* females versus control females (****P<0.0001 by χ^2 test; control, *n*=88; *Ube2i Zp3-cre+*, *n*=39). Scale bars: 40 µm. (J,K) Confocal *z*-stack projections of control (J) and *Ube2i Zp3-cre+* (K) oocytes collected after superovulation and stained for α-tubulin (green) and Hoechst (DNA) (blue). Scale bars: 20 µm. (L) Quantification of MI progression during *in vitro* culture of fully grown GV oocytes isolated from control and *Ube2i Zp3-cre+* mice over 8.5 h (**P=0.0077 by χ^2 test; (control, *n*=151; *Ube2i Zp3-cre+*, *n*=114). In panels C-F, data for individual animals are shown by black circles (control) or black triangles (*Ube2i Zp3-cre+*) with mean±s.e.m. shown. ns, not significant.

and meiotic progression. In this time frame, the majority of control oocytes progressed from GV to MI, but the progression of *Ube2i Zp3-cre+*oocytes was significantly altered (P=0.0077) (Fig. 1L). Similar percentages of oocytes died between genotypes (control, 5.3%; *Ube2i Zp3-cre+*, 8.8%) or reached pro-metaphase (control, 7.3%; *Ube2i Zp3-cre+*, 6.1%). However, the percentage of *Ube2i Zp3-cre+* oocytes that remained at the GV stage (27.2%) was nearly double that of control oocytes (14.6%), and control oocytes were also more successful at reaching MI (72.8%) than *Ube2i Zp3-cre+* oocytes (57.9%) (Fig. 1L). These data indicate that *Ube2i Zp3-cre+* oocytes have reduced meiotic competence compared with that of control oocytes.

In vitro-matured MI oocytes were further analyzed for spindle architecture and chromosome alignment by confocal microscopy using anti-α-tubulin antibodies for microtubules and Hoechst 33342 (hereafter, 'Hoechst') to detect DNA. For classification,

Development (2023) 150, dev201535. doi:10.1242/dev.201535

oocytes with multiple chromosomes lagging or not aligned on the metaphase plate were classified as having 'poor' alignment, whereas oocytes with all or nearly all chromosomes aligned at the metaphase plate were classified as having 'good' alignment. The majority of control MI oocytes had good chromosome alignment (81.2%) (Fig. 2A-C,G). In contrast, most of *Ube2i Zp3-cre+* MI oocytes had poorly aligned chromosomes (60.6%; $P<0.0001$) (Fig. 2D-G). In addition to misaligned chromosomes, *Ube2i Zp3-cre+* oocytes often displayed abnormal spindles, including those that appear stretched, shortened or disorganized (Fig. 2D-F). To quantify differences in spindle length and width, MI spindles were measured from pole to pole and at the widest point of the mid-spindle. *Ube2i Zp3-cre+* spindles were significantly shorter ($P=0.0444$) and narrower ($P=0.0285$) than control MI spindles (Fig. 2H,I). Chromosome spreads from *in vitro*-matured MI oocytes showed that *Ube2i Zp3-cre+* oocytes successfully formed bivalents; however, they appeared less condensed (Fig. 2J,K).

Because of the misaligned chromosomes, we further analyzed whether microtubule attachment to kinetochores was disrupted in *Ube2i Zp3-cre+* oocytes. We used a cold-stable assay as low temperatures depolymerize microtubules not attached to kinetochores, whereas microtubules attached to kinetochores are relatively stable (Ma and Schultz, 2013). Fully grown, prophase I-arrested GV oocytes (stripped of cumulus cells) were cultured to mid-MI (7 h), then placed in ice-cold minimum essential medium (MEM) prior to fixation and analyzed for microtubules (α-tubulin) and kinetochores (CREST). Owing to the abnormal chromosome structure and poor alignment in *Ube2i Zp3-cre+* oocytes at MI (Fig. 2), it was not possible to determine the precise number of kinetochore-microtubule attachments, so only the presence or absence of cold-stable microtubules was scored. Control oocytes were significantly more likely to have cold-stable microtubules (97.2%) than *Ube2i Zp3-cre+* oocytes (79.2%, $P=0.0333$) (Fig. 3A-C). Because of the impaired kinetochore-microtubule interaction in *Ube2i Zp3-cre+* oocytes, we further analyzed for changes in acetylation of histone H4 at lysine 16 (H4K16ac), as this histone modification maintains kinetochore function in somatic cells and possibly also in oocytes (Choy et al., 2011; Ma and Schultz, 2013). Fully grown control and *Ube2i Zp3-cre+* oocytes were analyzed at GV (Fig. 3D-F), pro-metaphase (Fig. 3G-I) and MI (Fig. 3J-L) stages by immunofluorescence and the signals quantified by confocal microscopy. The relative

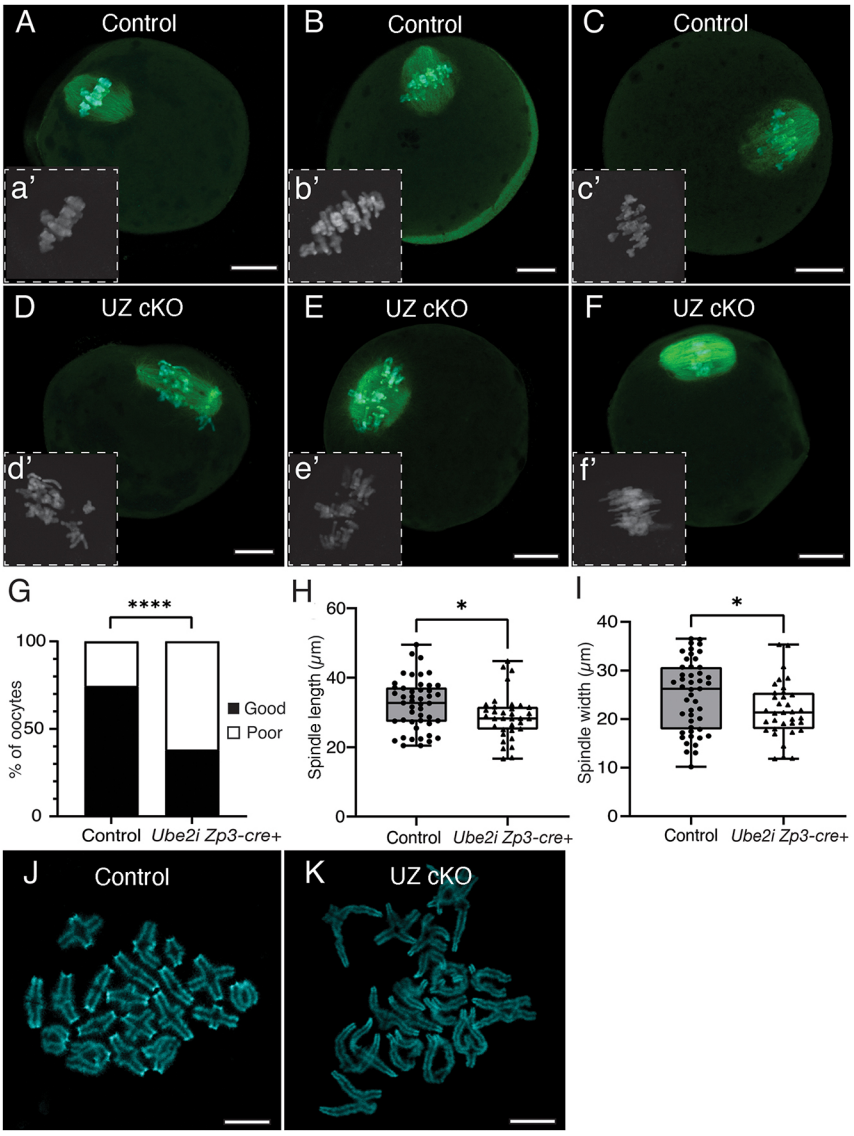

Fig. 2. *Ube2i Zp3-cre+* oocytes have misaligned chromosomes and abnormal spindles at MI. (A-F) Fully grown GV oocytes were cultured in CZB medium supplemented with glutamine for 8.5 h, then immunostained with anti-α-tubulin (green) antibody and stained with Hoechst for chromosome alignment. Representative confocal *z*-slices of control (A-C) and *Ube2i Zp3-cre+* ('UZ cKO') (D-F) oocyte MI spindles, with insets (a′-f′) showing chromosomes by Hoechst staining. Scale bars: 20 µm. (G) Quantification of chromosome alignment as determined by chromosome localization on the metaphase plate. ****$P<0.001$, Fisher's exact test; control, $n=110$; *Ube2i Zp3-cre+*, $n=66$. (H) MI spindle length measured from pole to pole of the bivalent spindle. *$P=0.0444$, unpaired two-tailed *t*-test; control, $n=47$; *Ube2i Zp3-cre+*, $n=35$. (I) MI spindle width measured at the widest point of the bivalent spindle. *$P=0.0285$ by unpaired two-tailed *t*-test; control, $n=47$; *Ube2i Zp3-cre+*, $n=35$. (J,K) Representative chromosome spreads (of 16 spreads of each genotype) showing MI bivalents from control MI oocytes (J) and less condensed MI bivalents from *Ube2i Zp3-cre+* MI oocytes (K). Scale bars: 10 µm.

Development (2023) 150, dev201535. doi:10.1242/dev.201535

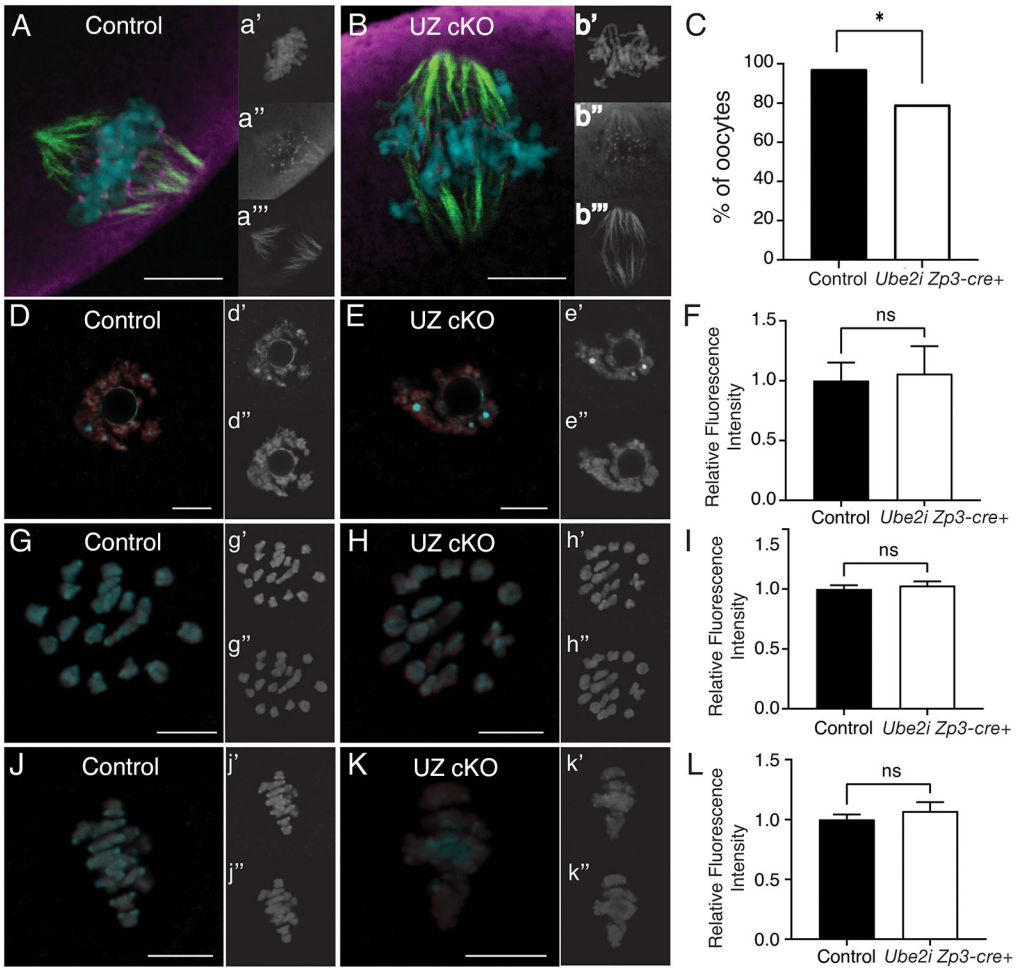

Fig. 3. *Ube2i Zp3-cre*+ MI oocytes have reduced kinetochore function but similar levels of H4K16ac as control MI oocytes. Fully grown, GV oocytes were cultured for 7 h, then placed in ice-cold MEM for 10 min to depolymerize non-kinetochore microtubules. Oocytes were stained for α-tubulin (green), CREST to mark kinetochores (magenta) and DNA (blue). (A,B) Merged images of projected representative confocal *z*-slices of a control (A) or *Ube2i Zp3-cre*+ ('UZ cKO') (B) cold-treated MI oocyte; unmerged panels are shown in a′,b′ (Hoechst), a″,b″ (centromere) and a‴,b‴ (α-tubulin). Scale bars: 10 µm. (C) Quantification of cold-treated oocytes with cold-stable microtubules present, shown as percentage of total oocytes analyzed (**P*=0.0333 by Fisher's exact test; control, *n*=36; *Ube2i Zp3-cre*+, *n*=24). (D,E,G,H,J,K) Analysis of H4K16ac immunostaining during MI progression. GV oocytes were collected and fixed immediately (GV stage, D,E), cultured to pro-metaphase (G,H) or MI (J,K), then were fixed and stained for H4K16ac (red) and DNA (Hoechst, blue). Merged images of representative *z*-slices for H4K16ac immunoreactivity (red) in control (D,G,J) and *Ube2i Zp3-cre*+ (E,H,K) oocytes. Unmerged panels are shown in d′-k′ (Hoechst) and d″-k″ (H4K16ac). (F,I,L) Quantification of positive H4K16ac signal showed no difference in the relative amount of H4K16ac at the GV (F) (control, *n*=35; *Ube2i Zp3-cre*+, *n*=29; *P*>0.05), pro-metaphase (I) (control, *n*=24; *Ube2i Zp3-cre*+, *n*=36; *P*>0.05) or MI (L) (control, *n*= 30; *Ube2i Zp3-cre*+, *n*=25) stages. All scale bars: 10 µm. Statistical analyses by unpaired two-tailed *t*-test. ns, not significant.

amount of H4K16ac was unchanged between genotypes at any stage, indicating that *Ube2i Zp3-cre*+ oocytes have reduced kinetochore function than control oocytes, which is not due to differences in H4K16ac levels at the GV, pro-metaphase or MI stages.

Fully grown *Ube2i Zp3-cre*+ GV oocytes fail to remodel chromatin and silence transcription

Prior to meiotic resumption, fully grown, prophase I-arrested GV oocytes undergo chromatin remodeling, which changes the configuration of the chromatin around the nucleolus. This change involves the transition from a less compact, non-surrounded nucleolus ('NSN') configuration, to a more compact, surrounded nucleolus ('SN') configuration (Mattson and Albertini, 1990; Debey et al., 1993; Ma et al., 2013). In isolated fully grown GV oocytes, the majority (87%) of control oocytes were in the SN configuration as expected (Fig. 4A,B,E). Compared with control oocytes, significantly fewer *Ube2i Zp3-cre*+ oocytes were in the SN configuration (18%) (Fig. 4C-E, $P<0.0001$). No difference in oocyte diameter was found between control and *Ube2i Zp3-cre*+ samples (Fig. 4F); thus, the difference cannot be attributed to *Ube2i Zp3-cre*+ oocytes not reaching a fully grown oocyte size. The transition from NSN to SN is also associated with transcriptional silencing (Ma et al., 2013), and thus we analyzed transcriptional activity of control and *Ube2i Zp3-cre*+ oocytes using 5-ethynyl-uridine (5EU) labeling. As expected, fully grown control GV oocytes in the SN configuration showed no fluorescent 5EU signal, (Fig. 5A), whereas control NSN oocytes had a positive fluorescent signal (Fig. 5B). Both transcriptionally active and inactive *Ube2i Zp3-cre*+ oocytes were identified (Fig. 5C,D), but there was a significantly higher proportion of *Ube2i Zp3-cre*+ oocytes that were transcriptionally active (77%, $P<0.0001$) compared with similar sized control oocytes (28%) (Fig. 5E,F), suggesting that *Ube2i Zp3-cre*+ oocytes fail to suppress transcription.

Development (2023) 150, dev201535. doi:10.1242/dev.201535

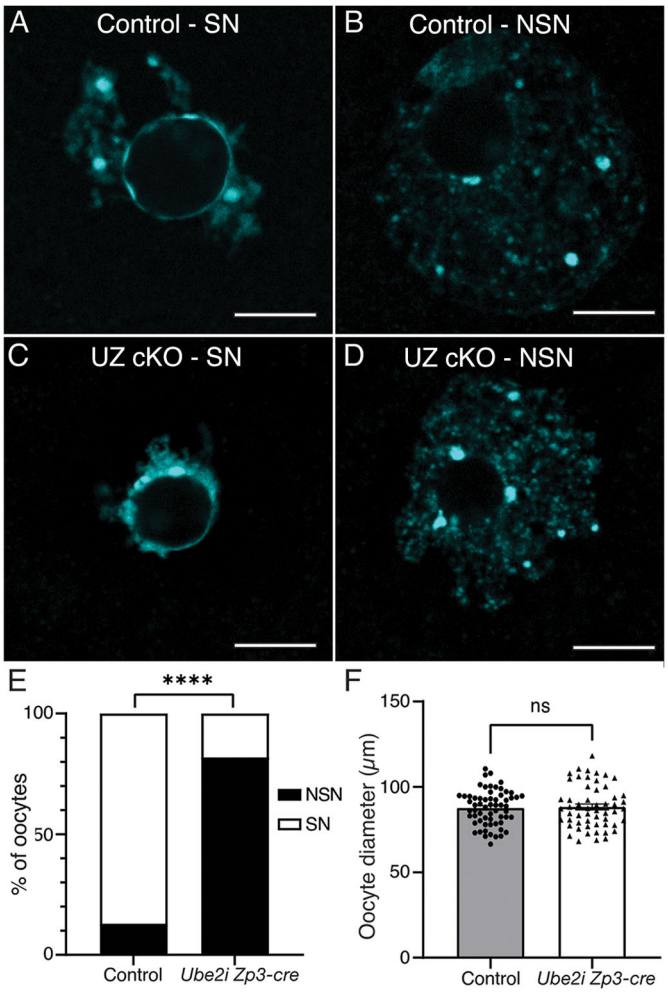

Fig. 4. *Ube2i Zp3-cre*+ GV oocytes fail to condense chromatin. (A-D) Control and *Ube2i Zp3-cre*+ GV oocytes were collected, fixed and stained with Hoechst for DNA configuration. Oocytes with a solid ring of DNA around the nucleolus were classified as having a surrounded nucleolus (SN) and oocytes lacking or with a partial ring of DNA were classified as having a non-surrounded nucleolus (NSN). Representative confocal *z*-slices of control oocytes with SN (A) and NSN (B) and of chromatin in *Ube2i Zp3-cre*+ ('UZ cKO') oocytes in SN (C) and NSN (D) configurations are shown. Scale bars: 10 µm. (E) Quantification of SN and NSN oocytes for each genotype (****P<0.0001, Fisher's exact test; control, n=47; *Ube2i Zp3-cre*+, n=46). (F) Verification of similar oocyte size for the samples used for quantification in E. Individual oocyte measurements, shown as circles (control, n=47) and triangles (*Ube2i Zp3-cre*+, n=46), show no difference in oocyte diameter between genotypes (ns, not significant by Fisher's exact test).

Histone modifications such as methylation are associated with transcriptional activity in GV oocytes, and trimethylation of histone H3 at lysine 3 (H3K4me3) and lysine 9 (H3K9me3) in mouse oocytes are markers of transcriptional repression (Smith et al., 2022). Because of the active transcription observed in *Ube2i Zp3-cre*+ oocytes (Fig. 5), we analyzed overall H3K4me3 and H3K9me3 levels in fully grown, prophase I-arrested GV oocytes by immunofluorescence (Fig. 6). Compared with control GV oocytes, *Ube2i Zp3-cre*+ GV oocytes had significantly reduced levels of both H3K4me3 (34%, P<0.0001, Fig. 6A-C) and H3K9me3 (27%, P<0.0001, Fig. 6D-F), supporting the lack of transcriptional repression in the mutant oocytes.

Ube2i Zp3-cre+ GV oocytes have a significantly altered transcriptome

Because *Ube2i Zp3-cre*+ fully grown, prophase I-arrested oocytes fail to silence transcription, we performed RNA sequencing of individual fully grown, prophase I-arrested oocytes from control and *Ube2i Zp3-cre*+ mice (n=17 oocytes per genotype) to determine changes in the transcriptome. Principal component analysis (PCA) identified two groups with 70% variance in principal component (PC) 1 (PC1), which readily separated the samples by genotype; 15% variance was explained by PC2, which showed a wider sample spread for *Ube2i Zp3-cre*+ oocytes than for control oocytes (Fig. 7A). Using a cutoff of $|\log_2(\text{fold change or FC})|\geq 1$ and adjusted P-value (P_{adj})<0.05, we identified 7603 differentially expressed genes (DEGs) in *Ube2i Zp3-cre*+ oocytes compared with control oocytes (Fig. 7B; Table S1). Of these DEGs, more upregulated genes (6308) were found compared with the number of downregulated genes (1295). To investigate biological functions associated with the DEGs, Gene Ontology (GO) analysis was performed for upregulated and downregulated DEGs (Sherman et al., 2022). Separate analysis of either upregulated and downregulated genes returned the same top GO term: 'regulation of transcription from RNA polymerase II promoter'. Differentially upregulated genes also returned the GO terms 'signal transduction', 'multicellular organism development', 'cell differentiation' and 'cell adhesion', whereas downregulated genes returned the GO terms 'positive regulation of transcription from RNA polymerase II promoter', 'multicellular organism development', 'cell differentiation' and 'DNA-templated regulation of transcription' (Fig. 7C).

Key oocyte-expressed genes were differentially regulated in *Ube2i Zp3-cre*+ fully grown, prophase I-arrested oocytes (Fig. 8A). Genes downregulated in *Ube2i Zp3-cre*+ oocytes included *Bmp15*, *Gdf9*, *H1oo* (also known as *H1f8*), *Hormad1*, *Mater* (or *Mlrp5*), *Msy2* (*Ybx2*), *Npm2*, *Oosp1*, *Rfpl4*, *Tgfb2*, *Zar1*, *Zp1*, *Zp2* and *Zp3*, whereas upregulated genes include *Blimp1* (*Prdm1*), *Pou5f1* (*Oct4*) and *Trim28*. Of note, both *Bmp15* and *Gdf9* are also significantly downregulated in *Ube2i Gdf9-icre*+ ovaries (Rodriguez et al., 2019) and may contribute to a reduced proliferation of the cumulus cell layer in antral follicles of *Ube2i Zp3-cre*+ ovaries and the reduction in cumulus expansion (Figs S4-S6). The oocyte-specific transcription factor *Nobox* was significantly upregulated in *Ube2i Zp3-cre*+ oocytes (Fig. 8B). *Nobox* was the only oocyte-specific transcription factor found to be differentially regulated. As both H3K4me3 and H3K9me3 were downregulated in *Ube2i Zp3-cre*+ oocytes (Fig. 6), we examined the DEGs for changes to genes encoding histone lysine methyltransferases and demethylases. The methyltransferase genes that were upregulated in *Ube2i Zp3-cre*+ oocytes included *Kmt2e*, *Setd1b*, *Setdb1* and *Setdb2*, whereas *Setd1a*, *Smyd2* and *Suv39h2* were downregulated (Fig. S7A). The demethylase genes that were upregulated included *Kdm4b*, *Kdm4c*, *Kdm4dl*, *Kdm5a* and *Kdm5b*, whereas *Kdm2b* and *Kdm7a* were downregulated (Fig. S7B).

Major chromatin remodeling is not required for global transcriptional silencing in GV oocytes (De La Fuente et al., 2004). However, to verify that transcriptome changes were not simply due to persistence of the NSN configuration of mutant GV oocytes, the DEG list from *Ube2i Zp3-cre*+ oocytes was compared with gene expression profiles previously reported to be associated with SN and NSN oocytes (Ma et al., 2013). The genes downregulated in wild-type SN oocytes compared with their expression in wild-type NSN oocytes represent only 2% (152/7603) of the DEGs in the *Ube2i Zp3-cre*+ oocytes. Similarly, the

Development (2023) 150, dev201535. doi:10.1242/dev.201535

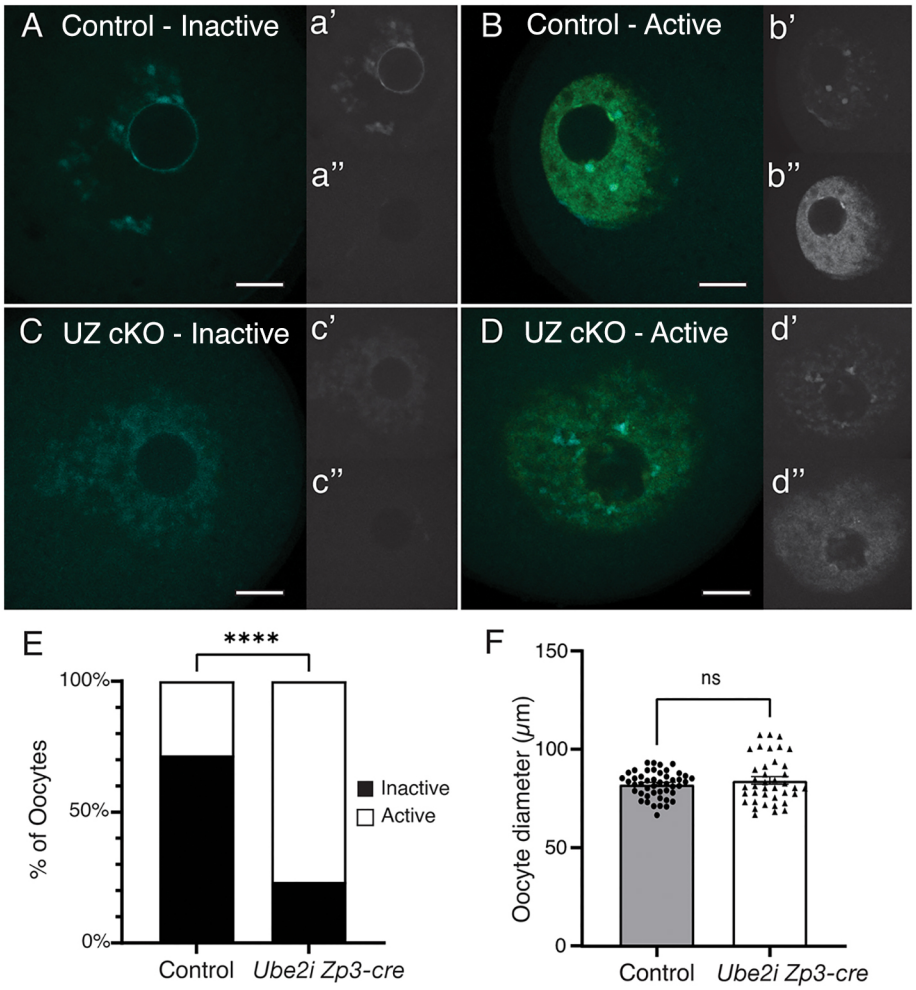

Fig. 5. *Ube2i Zp3-cre*+ GV oocytes fail to silence transcription. (A-D) Fully grown GV oocytes were held in meiotic arrest with milrinone and cultured for 2 min in the presence of 5EU to label newly synthesized RNA (positive transcriptional activity), shown in green. DNA was stained with Hoechst. Representative confocal *z*-slices of transcriptionally inactive oocytes from control (A) and *Ube2i Zp3-cre*+ ('UZ cKO') (C) mice, and of transcriptionally active oocytes from control (B) and *Ube2i Zp3-cre*+ (D) mice are shown for comparison. For the images in A-D, a′-d′ show DNA and a″-d″ show the 5-EU signal. Scale bars: 10 µm. (E) Quantification of inactive versus active transcription for each genotype (****P<0.001, Fisher's exact test; control, n=46; *Ube2i Zp3-cre*+, n=30). (F) Verification of similarity in oocyte size for samples used for quantification in E. Individual oocyte measurements, shown as circles (control, n=46) and triangles (*Ube2i Zp3-cre*+, n=30), show no difference in oocyte diameter between genotypes (ns, not significant by Fisher's exact test).

genes upregulated in wild-type SN oocytes compared with their expression in wild-type NSN oocytes comprise a mere 3% (226/7603) of the *Ube2i Zp3-cre*+ DEGs (Fig. S8). The overlapping genes are provided in Table S2. Thus, the predominance of NSN oocytes in *Ube2i Zp3-cre*+ oocytes is unlikely to fully explain the large transcriptomic changes in the mutant *Ube2i Zp3-cre*+ oocytes.

Loss of *Ube2i* in oocytes results in the upregulation of genes typically associated with ZGA

To further analyze the differences in gene expression, Ingenuity Pathway Analysis (IPA) (https://digitalinsights.qiagen.com/IPA) of the DEGs was used to identify the top upstream regulators. This analysis revealed that several of the top upstream regulators were associated with ZGA, including *Dppa2*, *Dppa4*, *Dux*, *Sox2* and Zscan4 genes (Fig. 8C) (Kramer et al., 2014). In the RNA-sequencing (RNA-seq) dataset, *Dppa4* expression was significantly decreased in *Ube2i Zp3-cre*+ oocytes (FC=−3.8; P<0.0001), whereas the expression levels of *Duxf3* (FC=+203.2; P<0.0001) and *Zscan4c* (FC +14.3; P<0.0001,) as well as those of *Zscan4a*, *Zscan4b*, *Zscan4d*, *Zscan4e and Zscan4af* were significantly increased; *Dppa2* (FC=0.96; P=0.7) and *Sox2* (FC=2.4; P=0.08) expression was unchanged between genotypes. Expression of the ZGA-associated genes, *Duxf3* and *Zscan4*, was validated in independent samples of fully grown, prophase I-arrested control and *Ube2i Zp3-cre*+ GV oocytes by RT-qPCR, confirming that these genes were upregulated in *Ube2i Zp3-cre*+ oocytes compared with control oocytes (Fig. S9). Other ZGA-associated genes such as *Eif1a*, encoding an embryonic transcription factor, and *Tmem92*, encoding a downstream target of ZSCAN4, had significantly higher expression as seen in the list of DEGs from the RNA-seq dataset as well as with RT-qPCR validation (Fig. S8).

In mice, ZGA occurs in two waves: the minor ZGA beginning in the S phase of one-cell embryos, and the major ZGA beginning from mid to late two-cell stage (Aoki, 2022). Comprehensive transcriptome analysis of MII, one-cell-stage and two-cell-stage embryos by RNA-seq previously identified five classes of genes according to changes in expression during progression of MII to two-cell embryos (Abe et al., 2018). We used informatic analysis to overlap our DEGs with the published major ZGA genes (clusters 1 and 2), minor and major ZGA genes (cluster 4), and minor ZGA genes (cluster 5) [gene sets derived from the DNA Data Bank of Japan (DDBJ) Sequence Read Archive accession number DRA006557; Abe et al., 2018]. Overlapping gene sets with a $|\log_2 FC| \geq 1$ and P_{adj}<0.05 are provided in Table S3. For genes associated with the minor ZGA (cluster 5), 20.0% of our DEGs were upregulated, whereas 5.6% were downregulated. For genes associated with the major ZGA (clusters 1 and 2), 13.2% of our DEGs were upregulated and 3.1% were downregulated. Finally, for the cluster associated with both minor and major ZGA (cluster 4), 23.7% of our DEGs were upregulated and 3.5% were downregulated. Thus, there was unexpected upregulation of over 17% of the ZGA-associated genes when *Ube2i* was conditionally

Development (2023) 150, dev201535. doi:10.1242/dev.201535

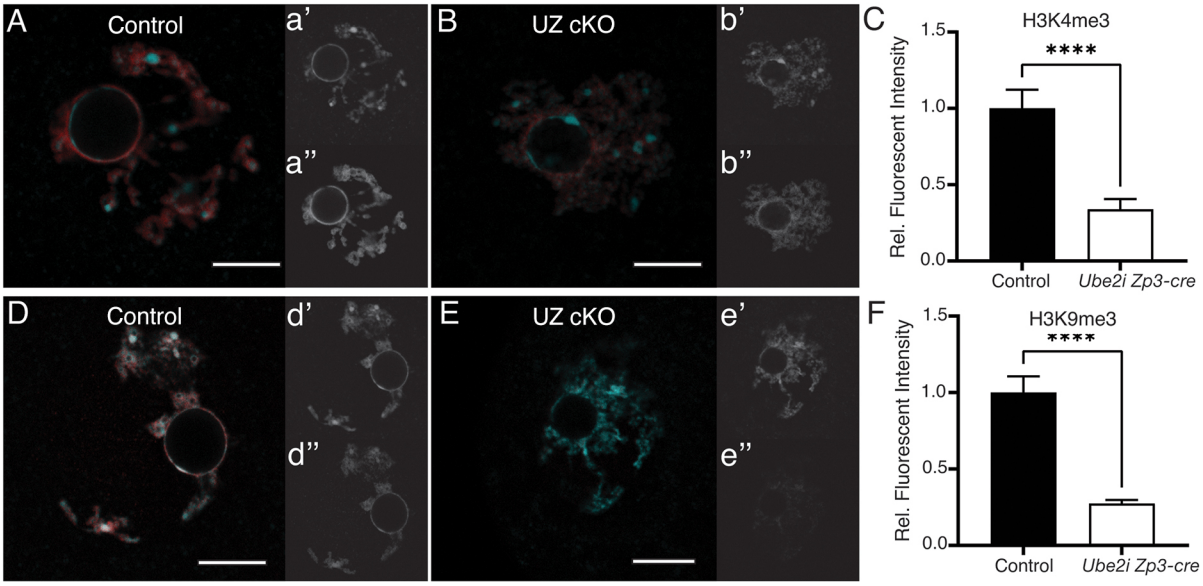

Fig. 6. The repressive histone modifications H3K4me3 and H3K9me3 are significantly decreased in *Ube2i Zp3-cre*+ oocytes. (A,B,D,E,) Control and *Ube2i Zp3-cre*+ GV oocytes were collected and immunostained for H3K4me3 (top row) or H3K9me3 (bottom row) and counterstained for DNA (Hoechst) (blue). (A) Merged images of representative confocal *z*-slices for H3K4me3 (A,B) and H3K9me (D,E) immunoreactivity (red) in control (A,D) and *Ube2i Zp3-cre*+ ('UZ cKO') (B,E) oocytes counterstained with Hoechst (blue); unmerged panels are shown in a′,b′,d′,e′ (Hoechst), a″,b″ (H3K4me3) and d″,e″ (H3K9me3). Scale bars: 10 µm. (C) Quantification of positive H3K4me3 shown as mean (±s.e.m.) relative fluorescence intensity (****P<0.0001 by unpaired two-tailed *t*-test; control, n=31 oocytes; *Ube2i Zp3-cre*+, n=30 oocytes). (F) Quantification of H3K9me3 signal showed that immunoreactivity was significantly reduced in *Ube2i Zp3-cre*+ oocytes (****P<0.0001 by unpaired two-tailed *t*-test; control, n=31 oocytes; *Ube2i Zp3-cre*+, n=28 oocytes).

deleted from oocytes in growing follicles. To further examine the overlap between our DEG list sorted by minor ZGA, minor and major ZGA, and major ZGA clusters, we performed IPA on the genes that were upregulated or downregulated in the *Ube2i Zp3-cre*+ oocytes (treatment versus control, $|\log_2 FC| \geq 1$ and $P_{adj} < 0.05$), and upstream transcription factors were identified and clustered with QIAGEN IPA and further annotated with PANTHER GO enrichment analysis (http://geneontology.org/). (Fig. 8D). Of these transcription factors, MYC had the higher number of affected downstream transcriptional target genes, followed by β-catenin (CTNNB1), huntingtin (HTT), TP63 (TRP63) and sex-determining region box 2 (SOX2). (Fig. 8D).

During ZGA, there is a transient upregulation of retrotransposons linked to totipotency (Low et al., 2021). The murine endogenous retrovirus-like gene *MuERV-L* (*Erv4*) is one of the earliest transcribed genes in mouse one-cell-stage embryos and a key target of the transcription factor DUX during ZGA (Kigami et al., 2003; De Iaco et al., 2017; Hendrickson et al., 2017). *MuERV-L* expression was analyzed by RT-qPCR and found to be significantly upregulated in *Ube2i Zp3-cre*+ oocytes (4014% compared with its expression in control oocytes, P<0.0001, Fig. S9) (Kigami et al., 2003). We additionally determined whether expression of other types of transposable elements (TEs) was altered using $|FC| \geq 2$ and false discovery rate (FDR)-adjusted P-value≤0.05. Eleven of 594 TEs were downregulated, whereas 583 TEs were upregulated. All major groups of retrotransposons, including long interspersed nuclear elements (LINEs), short interspersed nuclear elements (SINEs) and long terminal repeats (LTRs), were significantly upregulated (Fig. 9A) in fully grown, *Ube2i Zp3cre*+ GV oocytes compared with controls. Thus, the increase in the expression of genes associated with ZGA along with activation of TEs, including key retrotransposons, indicate that there are major disruptions in transcriptional regulation in the GV oocytes that arise by the end of folliculogenesis.

Based on the DEGs found to be associated with the minor and major ZGA, as well as the increase in TE activation that have previously been correlated to the two-cell stage (Evsikov et al., 2004), we compared our RNA-seq data from *Ube2i Zp3cre*+ and control oocytes with the previously published RNA-seq data from wild-type GV oocytes, early two-cell-stage and late two-cell stage (Zhang et al., 2016). Similar to the PCA for control versus *Ube2i Zp3cre*+ oocytes (Fig. 7A), these samples again clustered with 54% variance in PC1 and 26% variance in PC2 (Fig. 9B). The control samples readily clustered with the published GV dataset (Fig. 9B). In contrast, the *Ube2i Zp3cre*+ oocytes clustered independently in a range along PC1 between the GV stage and the early two-cell stage to the late two-cell stage, although, along PC2, they were clearly not GV, early two-cell stage or late two-cell stage (Fig. 9B). In total, the increase of genes associated with ZGA along with activation of TEs and the lack of clustering with GV oocytes indicate that by the end of folliculogenesis, there are major disruptions in transcriptional regulation in the fully grown *Ube2i Zp3cre*+ oocytes and a potential loss of cell identity.

DISCUSSION

The scope of regulation provided by SUMOylation in mammalian oocyte biology is not well known, particularly during oocyte growth within ovarian follicles. During folliculogenesis, critical hallmarks of oocyte development are established, including acquisition of meiotic and developmental competence. Towards the end of folliculogenesis, there is a major change in chromatin organization (NSN to SN), with the SN configuration associated with global suppression of transcription and increased developmental competence (Mattson and Albertini, 1990; Zuccotti et al., 1998; Bouniol-Baly et al., 1999; De La Fuente and Eppig, 2001; Miyara et al., 2003). Although SUMOylation is known to be a key process for transcriptional repression in general (Ouyang and Gill, 2009; Theurillat et al., 2020), a role for

Development (2023) 150, dev201535. doi:10.1242/dev.201535

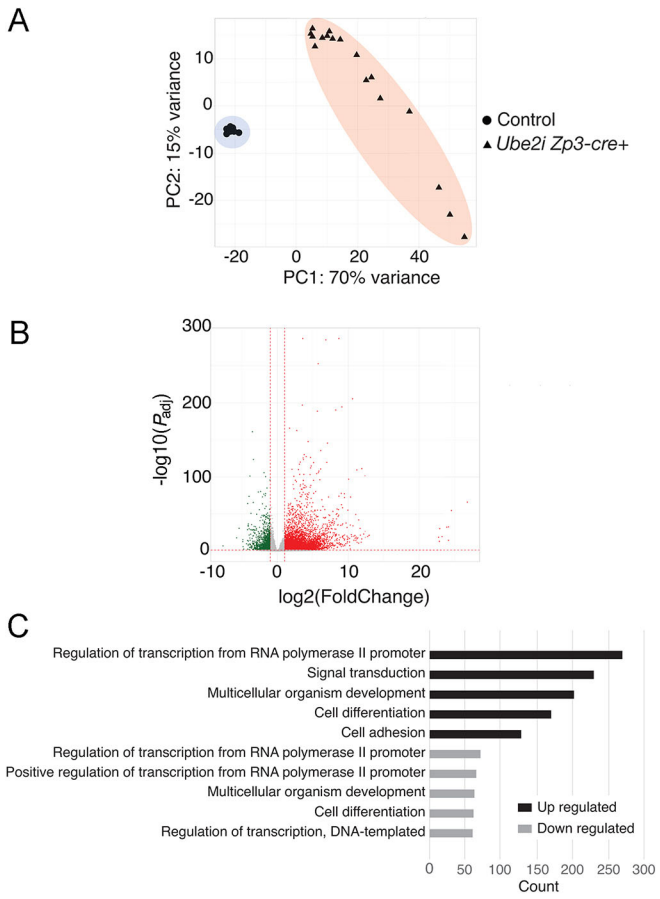

Fig. 7. *Ube2i Zp3-cre*+ oocytes have a significantly altered transcriptome. (A) PCA plot of transcriptomes of control (*n*=17) and *Ube2i Zp3-cre*+ (*n*=17) fully grown GV oocytes. Circles represent control oocytes and triangles represent *Ube2i Zp3-cre*+ GV oocytes. The shading (blue or peach) is provided to delineate the two comparison groups (control versus oocyte conditional knockout, respectively). (B) Volcano plot showing DEGs in control and *Ube2i Zp3-cre*+ GV oocytes from RNA sequencing of individual oocytes. (C) GO analysis of DEGs with a twofold increase or a twofold decrease (P<0.05).

SUMOylation for global transcriptional repression in mammalian oocytes has not been previously described. Using a novel mouse model developed to delete *Ube2i* selectively in growing oocytes, we demonstrate that UBE2I is necessary for the processes of chromatin remodeling, transcriptional regulation and differentiation into fully grown GV oocytes, in addition to its more well-known roles in meiotic progression (Fig. S10).

The oocyte-specific knockout of *Ube2i* using *Gdf9-icre* demonstrated that *Ube2i* was required for stability of the ovarian reserve (Rodriguez et al., 2019). It was unclear if accelerated depletion of the ovarian reserve was due to direct effects of *Ube2i* in oocytes of primordial follicles or indirectly due to loss of growing follicles, which produce factors, including anti-Müllerian hormone, that regulate primordial follicle dynamics (Durlinger et al., 1999; Pangas, 2012). To test this, we used the oocyte-deleter strain *Zp3-cre*, which is temporally distinct from *Gdf9-icre* (Lan et al., 2004). Even though deletion at the primordial stage (*Ube2i Gdf9-icre*+) or from primary follicles onward (*Ube2i Zp3-cre*+) caused female sterility and oocyte arrest at MI, unlike *Ube2i Gdf9-icre*+ ovaries, *Ube2i Zp3-cre*+ ovaries showed a stable primordial follicle pool with limited effects on overall follicle populations. Thus, *Ube2i* has essential roles in oocytes of both primordial follicles and growing follicles. A detailed comparison of phenotypes is shown in Table S4.

Although the number of follicles at most stages of folliculogenesis were unchanged even in 6-month-old *Ube2i Gdf9-icre*+ mice, there was a 30% decline in primary follicles and alterations in growth of the cumulus cell layer surrounding oocytes, which resulted in a smaller area of cumulus cell expansion following ovulation in *Ube2i Gdf9-icre*+ mice compared with that in controls. This secondary effect on cumulus cells may reflect reductions in the oocyte-expressed genes *Bmp15* and *Gdf9*. BMP15 and GDF9 function in a complex signaling loop that bidirectionally regulates oocyte and cumulus cell development, which includes maintaining meiotic arrest (Su et al., 2004; Peng et al., 2013; Wigglesworth et al., 2013). Even though the cumulus cell layer was reduced in *Ube2i Gdf9-icre*+ oocytes, it appeared to be sufficient to maintain bidirectional communication, as oocytes from *Ube2i Gdf9-icre*+ grew to a similar size as control oocytes and maintained meiotic arrest; additionally, *Ube2i Gdf9-icre*+ ovaries lacked hallmarks of severe cumulus cell defects that lead to follicle and oocyte loss (Pangas et al., 2006; Ploutarchou et al., 2015). More detailed experiments are required to understand the reduction in primary follicles and changes to cumulus cell growth that can impact oocyte quality.

In wild-type ovaries, by the end of folliculogenesis, a significant proportion of fully grown oocytes are in the SN configuration, with the remainder in NSN (Zuccotti et al., 1995). Although NSN oocytes resume meiosis normally, progress to MII and can be fertilized, they subsequently arrest at the two-cell stage (Zuccotti et al., 1998). The majority of *Ube2i Zp3-cre*+ GV oocytes fail to transition from the NSN to SN chromatin configuration; however, unlike wild-type NSN oocytes or other mutant mouse lines that retain high levels of NSN oocytes in antral follicles (Burns et al., 2003), *Ube2i Zp3-cre*+ GV have a twofold reduction in meiotic resumption. This suggests that the defects in *Ube2i Zp3-cre*+ are not solely due to the presence of the NSN stage. Of the oocyte-expressed genes downregulated in *Ube2i Zp3-cre*+, several have knockout mouse models that show an increased percentage of GV oocytes in the NSN configuration. These includes germline knockouts of the maternal effect genes *Npm2* and *Mater*, which both show a later arrest (two-cell-stage embryo) compared with that of *Ube2i Zp3-cre*+ model (Tong et al., 2000; Burns et al., 2003; Monti et al., 2013). The maternal effect gene *Zar1*, for which the knockout mouse model arrests at the one-cell-stage embryo (Wu et al., 2003), is also downregulated in *Ube2i Zp3-cre*+ oocytes. During development, *Zar1* and *Mater* transcripts are degraded from GV to MII (Su et al., 2007), with 90% of all maternal-effect gene transcripts in oocytes degraded by ZGA (Schellander et al., 2007; Walser and Lipshitz, 2011). The decreased levels of maternal-effect gene transcripts, in spite of the maintenance of active transcription in *Ube2i Zp3-cre*+, may additionally suggest that RNA stability or storage of subsets of transcripts could be affected, although this remains to be determined. One hypothesis is this could be due in part to a reduction in the levels of the RNA-binding protein MSY2, which is significantly downregulated approximately twofold, as *Msy2*$^{-/-}$ GV oocytes have a 25% reduction in poly(A)-containing RNA (Medvedev et al., 2011). Other RNA-binding proteins (RBPs) are targets of SUMOylation or contain SUMO-interacting motifs (Richard et al., 2017; Ruta et al., 2021); however, the RBP SUMO targets in oocyte biology, which might include MSY2, remain to be characterized.

Although the NSN-to-SN chromatin configuration switch in fully grown oocytes is associated with transcriptional silencing, these

Development (2023) 150, dev201535. doi:10.1242/dev.201535

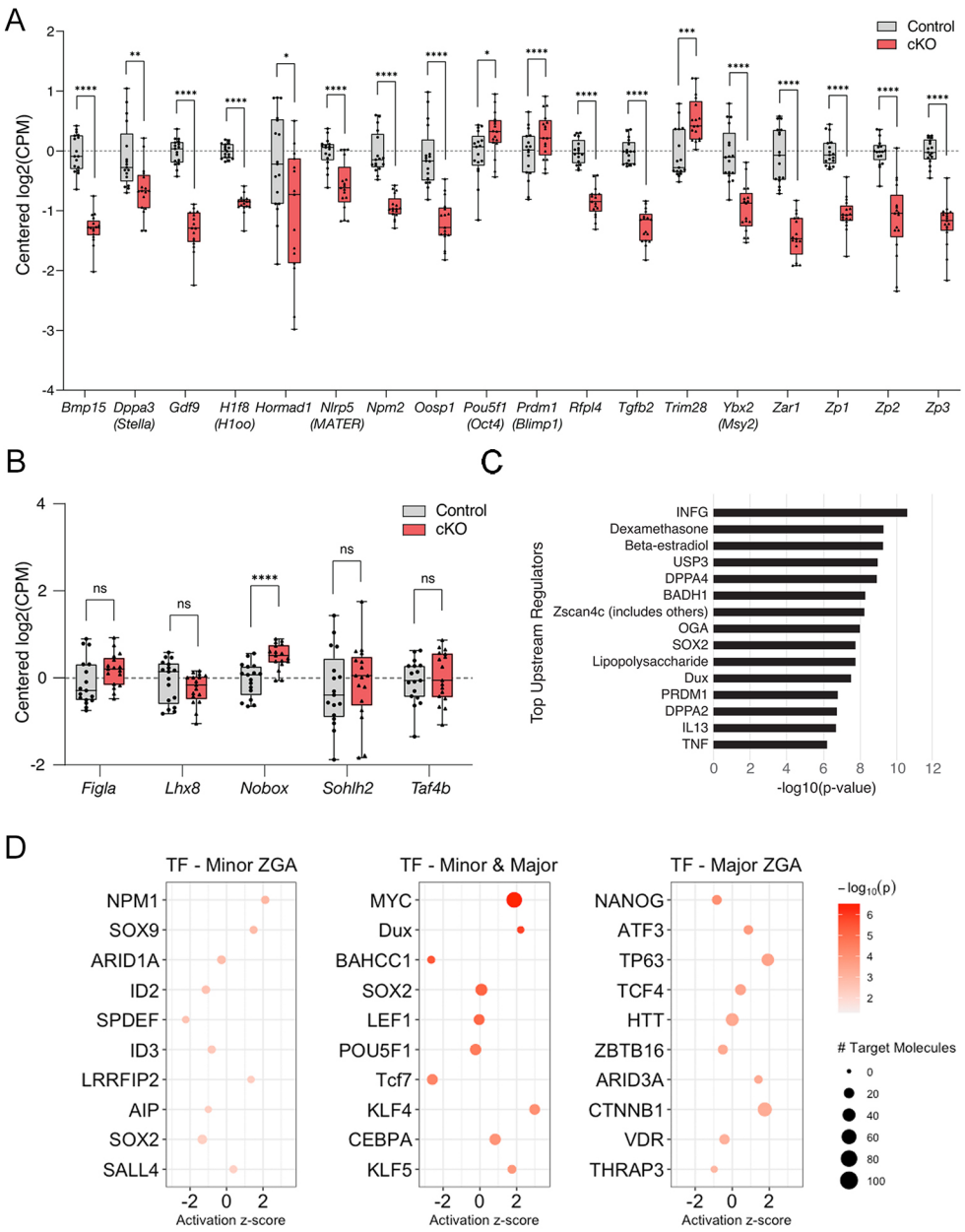

Fig. 8. Differentially expressed genes in *Ube2i Zp3-cre+* GV oocytes include oocyte-specific genes and maternal-effect genes. (A) Select genes known to be important in oocyte development and fertility had significantly altered expression levels in *Ube2i Zp3-cre+* ('cKO', red) fully grown GV oocytes compared with control (grey) fully grown GV oocytes from the RNA-seq analysis using DESeq2. Counts per million (CPM) values for the expression levels of each gene were normalized to those of the control and log transformed. (B) Expression levels of key oocyte transcription factors. In A,B, the boxes represent the 25-75th percentiles, whiskers extend to the minimum and maximum values, and the medians are marked with lines. The dotted lines represent the normalized log-transformed value (0). (C) Top upstream regulators determined from IPA of the DEG list derived from the RNA-seq data. (D) Enrichment plots of the top ten most significant upstream regulatory transcription factors (TFs) identified through IPA during the minor, major and minor, and major ZGA. Gene sets for comparison were derived from the DDBJ Sequence Read Archive accession number DRA006557 from clusters 1 and 2 (major), cluster 4 (minor and major), and cluster 5 (minor). ns, not significant; **P*<0.05; ***P*<0.01; ****P*<0.001; *****P*<0.0001.

processes can be uncoupled (Bouniol-Baly et al., 1999; De La Fuente et al., 2004; Ma et al., 2013) and mechanisms underlying transcriptional silencing are not well understood (Schultz et al., 2018). Transcriptional silencing in wild-type GV oocytes is associated with the accumulation of H3K4me3 and H3K9me3 (Kageyama et al., 2007; Chousal et al., 2018). *Ube2i Zp3-cre+* GV oocytes show loss of these repressive marks and a failure to silence transcription, potentially in part because they remain in the NSN configuration, but this could also suggest that SUMOylation plays a role in the establishment of trimethylated H3K4 and H3K9 during oocyte development. Decreased levels of H3K4me3 and H3K9me3 are also associated with expression of ZGA-associated genes such as the Zscan4 gene family (Smith et al., 2022). Active removal of H3K4me3 by the lysine demethylases KDM5A and KDM5B (both of which are significantly upregulated in *Ube2i Zp3cre+* oocytes) is required for ZGA, and reduction of these marks results in premature activation of the ZGA in GV oocytes (Dahl et al., 2016). Our informatic analysis of *Ube2i Zp3-cre+* GV oocyte DEG revealed the category of ZGA-associated genes as top upstream regulators, including MYC, a proposed master regulatory gene in the two-cell-stage embryo (Zeng and Schultz, 2005). The upregulation of genes typically associated with ZGA suggests that the fully grown *Ube2i Zp3cre+* oocytes had not acquired the appropriate differentiation state by the end of folliculogenesis or had an altered cell fate. SUMOylation is known to be involved in ZGA (Higuchi et al., 2019), but the upregulation of genes normally associated with ZGA is pathological in GV oocytes. Genes associated with ZGA in *Ube2i Zp3-cre+* GV oocytes (*Dux*, *Zscan4* and *Eif1a*-like genes) showed a similar upregulation when *Ube2i* was knocked down in embryonic stem cells, which converted embryonic stem cells to a more pluripotent, two-cell-embryo-like state (Cossec et al., 2018). The increase in genes associated with ZGA, along with activation of retrotransposons, suggests that the epigenetic program of oocytes either was not established during follicle development or, if established, was not maintained. Thus, our data support a hypothesis that SUMOylation in fully grown oocytes is required

Development (2023) 150, dev201535. doi:10.1242/dev.201535

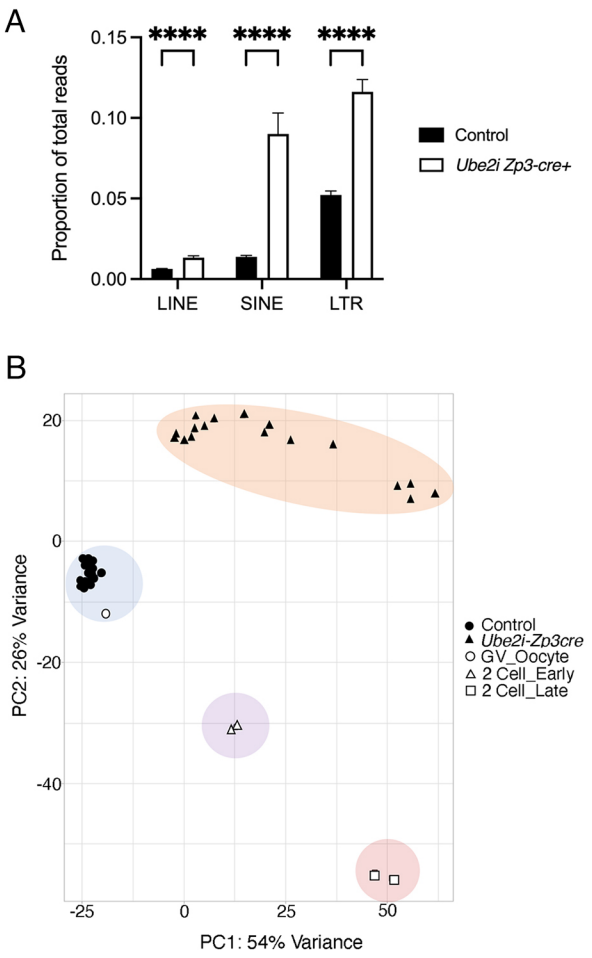

Fig. 9. *Ube2i Zp3-cre*+ fully grown GV oocytes show increased retrotransposon expression and an altered cell identity.
(A) Quantification of LINEs, SINEs, and LTRs identified with TEtranscripts v2.2.3 in the RNA-seq dataset comparing fully grown control GV oocytes with *Ube2i Zp3-cre*+ GV oocytes. Mean±s.e.m. is shown. ****P<0.0001, unpaired two-tailed *t*-test. (B) PCA plot of transcriptomes of control (n=17) and *Ube2i Zp3-cre*+ (n=17) oocytes, compared with published RNA-seq data of GV oocytes and early and late two-cell embryos, derived from GSE71434.

for the oocyte transcriptional program and SUMOylation may safeguard oocyte 'fate' or 'identity' until it is necessary to activate the zygotic genome, similar to its role in other cellular contexts (Cossec et al., 2018).

In summary, the phenotype of *Ube2i Zp3-cre*+ GV oocytes indicates new roles for UBE2I in oocytes during folliculogenesis, which are necessary for fertility. The phenotype includes loss of transcriptional silencing prior to meiotic resumption, improper chromatin remodeling at the end of folliculogenesis, decreased production or regulation of maternal-effect gene transcripts and loss of suppression of transcripts associated with totipotency (i.e. the two-cell stage). In terms of genetic regulation, the increase in gene expression associated with ZGA and upregulation of retrotransposons suggests that the epigenetic program of *Ube2i Zp3-cre*+oocytes is likely altered. Understanding these genetic changes in combination with the improper chromatin state will provide insight into how the oocyte maintains its own genetic program while preparing for early events in embryogenesis (Hanna et al., 2018).

MATERIALS AND METHODS

Experimental mice

Experimental procedures utilizing mice were performed in compliance with the National Institutes of Health Guide for the Care and Use of Laboratory Animals, and Institutional Animal Care and Use Committee-approved animal protocols at Baylor College of Medicine (AN-4762). The *Ube2i*$^{loxP/loxP}$ mice used in this study were previously generated and provided by Sean Hartig (Baylor College of Medicine, Houston, TX, USA) (Cox et al., 2021) and backcrossed to the F1 hybrid *C57BL/6J/129S7/SvEvBrd* background of our previous study (Rodriguez et al., 2019). Recombination by Cre generates a null allele through deletion of exons 3 and 4 as described (Cox et al., 2021). *Ube2i*$^{loxP/loxP}$ females were mated to *Zp3-cre* [strain *Tg(Zp3-cre)*$^{93Knw/J}$; The Jackson Laboratory, strain 003651] males to generate *Ube2i*$^{loxP/+}$ *Zp3-cre*+ males, which were then crossed to *Ube2i*$^{loxP/loxP}$ females to generate *Ube2i*$^{loxP/loxP}$ *Zp3-cre*+ females, called *Ube2i Zp3-cre*+ in text. All cre lines were maintained on the male line. Generation and oocyte-restricted expression of *Zp3-cre* mice as well as genotyping has been previously characterized (de Vries et al., 2000; Lan et al., 2004). Genomic DNA from ear punches was used for genotyping. Cre-negative female littermates (*Ube2i*$^{loxP/loxP}$) were used as controls in all experiments to minimize differences in genetic backgrounds. *Ube2i*$^{loxP/loxP}$ were also crossed to *Gdf9-icre*, and the sterility and ovarian follicle loss phenotype validated against the prior study (Rodriguez et al., 2019). Genotyping primers are listed in Table S5.

Fertility analysis

To test fecundity, sexually mature (6-week-old) *Ube2i Zp3-cre*+ females or control littermates were pair-housed with sexually mature (8-week-old) wild-type males of known fertility and continuously mated for 6 months (n=3 mating pairs per genotype). Females were monitored daily for new litters and the number of pups, date of birth and sex was recorded, similar to prior publications (Pangas et al., 2008; Rodriguez et al., 2019). Any resulting litters were weaned at 3 weeks of age.

Tissue collection, histological analysis and follicle quantification

Mice were anesthetized using isoflurane (Abbott Laboratories) inhalation and euthanized by cervical dislocation. Ovaries were collected and fixed in 10% neutral buffered formalin (Electron Microscopy Sciences) overnight, followed by standard paraffin processing and embedding at the Human Tissue Acquisition and Pathology Core at Baylor College of Medicine. Thirteen control ovaries (from 13 mice) and 12 *Ube2i Zp3-cre*+ ovaries (from 12 mice) were serially sectioned at 5 µm using an Ergostar HM200 microtome (Microm) and stained with periodic acid (Sigma-Aldrich) and Schiff's reagent (Sigma-Aldrich) (PAS) for analysis. Brightfield images were obtained using Axioscope 2 plus and Zeiss Zen Software v2.3 and Zen Blue. For morphometric quantification, ovaries were sectioned at 5 µm and the follicles in every fifth section were manually counted (Tilly, 2003). To avoid overcounting, only follicles with a visible oocyte nucleus were counted. For follicles smaller than the antral stage, a correction factor was applied by multiplying by 5 to estimate the number of total follicles (Hirshfield and Midgley, 1978; Tilly, 2003). Corpora lutea and antral follicles were counted in total by following each individually through serial images. Follicle classification was based on previous studies into primordial (type 2), primary (types 3a and 3b), secondary (type 4), preantral (types 5a and 5b) and antral (types 6-8) (Pedersen and Peters, 1968).

Hormone analysis

Blood was collected from isoflurane-anesthetized group-housed, 6-month-old mice by cardiac puncture, and the serum was separated by centrifugation in microtainer collection tubes (Becton, Dickinson, and Company) and frozen at −20°C until assayed. Mouse FSH and estradiol levels were analyzed by ELISA at the University of Virginia Ligand Core Facility [Specialized Cooperative Centers Program in Reproductive Research, National Institute of Child Health and Human Development (NICHD)/National Institutes of Health (NIH) U54-HD28934]. The assay method information is available online (https://med.virginia.edu/research-in-reproduction/ligand-assay-analysis-core/assay-methods/). Data were log

Development (2023) 150, dev201535. doi:10.1242/dev.201535

transformed before statistical analysis by Welch's two-tailed unpaired *t*-test (FSH) or two-tailed unpaired *t*-test (FSH).

Oocyte collection, culture and fixation

For analysis of cumulus-oocyte complexes or collection of oocytes following superovulation, female mice aged 5-6 weeks were injected with 5 IU pregnant mare's serum gonadotropin (PMSG; ProSpecBio), and 46 h later injected with 5 IU human chorionic gonadotropin (hCG; Pregnyl; Merck Pharmaceuticals). Mice were euthanized 16-18 h after injection with hCG and cumulus-oocyte complexes were harvested from the oviduct ampulla and imaged live, or incubated with 0.3 mg/ml hyaluronidase (Sigma-Aldrich) to detach cumulus cells, then the oocytes were fixed in 3.7% paraformaldehyde (PFA; Electron Microscopy Sciences) in 0.1% BSA (Sigma Aldrich) in PBS (BSA-PBS) for 15-20 min, then rinsed through five drops of BSA-PBS to prevent overfixation. Oocytes were stored in BSA-PBS at 4°C overnight, or directly used for immunostaining.

For collection of fully-grown, prophase I-arrested GV oocytes, 5- to 6-week-old female mice were injected with 5 IU PMSG and ovaries were excised after 44-46 h into M2 medium (Millipore Corporation) supplemented with 2.5 µM milrinone (Sigma Aldrich) to maintain prophase I meiotic arrest. Follicles were ruptured via puncturing with a 26G needle to release oocytes into the medium. Oocytes were denuded of cumulus cells via continuous pipetting (De La Fuente et al., 2004) and separated from cumulus cells by passing the medium through a 40 µm mesh strainer (oocytes were retained, whereas cumulus cells passed through the mesh strainer). Any remaining cumulus cells were mechanically stripped by gently pipetting the oocyte through a clinical IVF 'stripper pipettor' (Cooper Surgical) using a plastic pipette tip slightly smaller than the diameter of the oocyte. After denuding, oocytes were rinsed through ten drops of EmbryoMax CZB medium with Phenol Red (Millipore Corporation) supplemented with 2 mM L-glutamine (Thermo Fisher Scientific) to wash out milrinone and cultured in a fresh drop of medium covered with mineral oil (Sigma-Aldrich) at 37°C and 5% CO_2. Oocytes that had not undergone GVBD were removed from the culture after 2.5 h, and oocytes were cultured for 5 h to pro-metaphase I or 7.5-8 h to MI or for monitoring meiotic progression. After culturing to the desired stage, oocytes were fixed in 3.7% PFA in BSA-PBS for 15-20 min, then rinsed through five drops of BSA-PBS to prevent overfixation. Oocytes were stored in BSA-PBS at 4°C overnight, or directly used for immunostaining.

Chromosome spreads

Chromosomes spreads were performed similar to prior studies (El Yakoubi et al., 2017; Nguyen et al., 2018). Oocytes were collected and cultured to pro-metaphase (5 h) or MI (8.5 h), followed by the removal of the zona pellucida (ZP) by transferring the oocytes through up to ten drops of acid Tyrode's solution (Sigma-Aldrich) under a brightfield microscope until the ZP was visibly removed. After removal of the ZP, oocytes were rinsed through ten drops of M2 medium and returned to the incubator to recover for 30 min. Then, 50 µl of chromosome-spreading solution [0.64% PFA, 3 mM dithiothreitol (Thermo Fisher Scientific), 0.16% Triton X-100 (Thermo Fisher Scientific)] was applied to the wells of PTFE printed slides (VWR), and three to five oocytes were transferred to the well. Lysing of the oocytes was confirmed by visual monitoring using a brightfield microscope. The slides were allowed to dry at room temperature and stored at −20°C until use.

Immunostaining

Immunofluorescence was performed essentially as described previously (Rodriguez et al., 2019). After fixation, oocytes were permeabilized in 0.1% Triton X-100 in BSA-PBS for 20 min, then rinsed through five drops of BSA-PBS. Blocking was performed in 1.0% BSA and 0.01% Tween-20 for 45 min to 1 h at room temperature, or overnight at 4°C. Cells were incubated in primary antibody diluted in blocking buffer for 2 h, or overnight at 4°C, followed by three 10-min washes in BSA-PBS. After washing, oocytes were incubated in the secondary antibodies diluted in blocking buffer for 1 h, followed by three 10-min washes in BSA-PBS. DNA was stained using 20 µM Hoechst (Thermo Fisher Scientific) in BSA-PBS for 15 min, and briefly rinsed in BSA-PBS. Oocytes were mounted on Superfrost Plus glass slides (VWR) under no. 1.5 thickness coverglass (VWR) using ProLong Diamond Antifade Mount (Thermo Fisher Scientific) and allowed to dry overnight at room temperature. Slides were stored at 4°C until imaging. Information on antibodies used in this study can be found in Table S6.

Chromosome spreads were allowed to warm to room temperature, then rinsed three times in PBS. Blocking was performed with 3.0% BSA in PBS for 45 min. Primary antibodies were diluted in blocking buffer and incubated on the chromosome spreads for 2 h, followed by three 15-min washes with PBS. Secondary antibodies were diluted in blocking buffer and incubated on the spreads for 1 h, followed by PBS washes. DNA was then stained using 20 µM Hoechst for 15 min, followed by a PBS rinse. Negative controls were obtained by omitting the primary antibody, instead incubating in blocking buffer alone, before incubating in the secondary antibody diluted in blocking buffer. ProLong Diamond was applied to the samples, and a no. 1.5 coverslip was applied and allowed to dry at room temperature. Slides were stored at 4°C until imaged.

Confocal microscopy

Immunofluorescence images were obtained at the Optical Imaging and Vital Microscopy Core at Baylor College of Medicine on a Zeiss LSM 780 or 880 confocal microscope using the 40× oil objective. *Z*-stacks were captured using optimal step sizes from the bottom of the region of interest to the top of the region. To acquire images that were used for fluorescence quantification, the parameters were held consistent across all samples. *Z*-stacks were exported from Zeiss Zen 3.2 Blue edition and the signal intensity was measured using NIH ImageJ software. Negative controls were used to determine background fluorescence signal intensities, which were subsequently subtracted from the fluorescence intensities of the experimental oocytes.

Chromosome alignment analysis

Chromosome alignment was analyzed using oocytes cultured for 8.5 h and fixed as described above. Oocytes were then stained for α-tubulin and DNA, then *z*-stacks of the chromosomes were collected for analysis. MI chromosome alignment was performed in Zeiss Zen 3.2 Blue edition. Oocytes with all chromosomes within 5 µm of the metaphase plate were classified as 'good', whereas oocytes with one or more chromosomes more than 5 µm away from the metaphase plate were classified as 'poor'. To analyze SN and NSN chromosome configuration of GV oocytes, oocytes were collected, denuded and fixed, and DNA was stained with Hoechst. Oocytes with a solid ring of DNA around the nucleolus were classified as SN, whereas oocytes lacking a ring of DNA around the nucleolus or containing only a partial ring were classified as NSN. To ensure that immature oocytes were not used, oocyte diameter was measured across the midpoint of the oocyte, not including the ZP.

In vitro transcription assay

GV oocytes were collected as above and cultured in the presence of 2 mM 5-ethynyl uridine (5EU) (Click-IT RNA Alexa Fluor 488 Imaging Kit, Invitrogen) in EmbryoMax CZB medium supplemented with L-glutamine according to the manufacturer's recommended procedure. In brief, oocytes were cultured in 5EU for 45 min, then immediately fixed in 3.7% PFA for 20 min and rinsed through five drops of BSA-PBS. The oocytes were permeabilized with 0.1% Triton X-100 in BSA-PBS for 15 min, followed by BSA-PBS rinse. The Click-IT labeling reaction was performed by incubating the oocytes in the provided reaction cocktail according to the manufacturer's protocol. Oocytes were then counterstained with 20 µM Hoechst for 15 min, rinsed in BSA-PBS, mounted in ProLong Diamond and allowed to dry overnight. *Z*-stacks of each oocyte were obtained for analysis. Oocytes containing greater fluorescence signals than the signals in negative-control oocytes were considered to be transcriptionally active. To ensure that immature oocytes were not used, oocyte diameter was measured across the midpoint of the oocyte, not including the ZP.

Cold-stable assay

GV oocytes were collected and denuded, then cultured for 7 h in EmbryoMax CZB medium supplemented with L-glutamine. Oocytes were then placed in

Development (2023) 150, dev201535. doi:10.1242/dev.201535

ice-cold M2 medium (Invitrogen) for 10 min, fixed in 3.7% PFA for 20 min, then used in immunostaining (as above) for α-tubulin and kinetochores (anti-CREST).

RNA isolation and RT-qPCR

Denuded, fully grown GV oocytes were collected from PMSG-stimulated control and *Ube2i Zp3cre+* mice as independent pools as described above. Total RNA was generated using the PicoPure Isolation Kit (Applied Biosystems) and treated with DNase (QIAGEN) prior to the generation of cDNA. The average amount of RNA obtained per oocyte was 0.081 ng. 50 ng of RNA was used to generate cDNA using the High-Capacity RNA-to-cDNA reverse transcription kit (Invitrogen). cDNA was diluted 1:2 in water and 2 µl used for RT-qPCR. RT-qPCR was performed using the PowerUp SYBR Green Master Mix (Applied Biosystems) on an Applied Biosystems StepOnePlus real-time PCR system, with samples performed in duplicate. A melt-curve analysis was performed to verify that the primers amplified a single peak. Amplification of gene expression from RT-qPCR data was analyzed using the ΔΔCt method (Livak and Schmittgen, 2001) and normalized to ubiquitin C (*Ubc*) expression for each sample. In all graphs, the data are shown relative to the mean of the control value. The primers used for RT-qPCR are listed in Table S5.

RNA-seq and informatic analysis

The RNA-seq library was generated according to SMART-seq v4 Ultra low input RNA kit (Takara). In brief, the largest fully grown GV oocytes (n=17 oocytes per genotype) were collected from five control and five *Ube2i Zp3-cre+* PMSG-primed females and were lysed in lysis buffer (Takara Bio), 3-SMART-seq CDS primer II (Takara Bio) and V4 oligonucleotide (Takara Bio) were added for first-stranded cDNA synthesis and stored at −80°C until cDNA was generated. cDNA was amplified using PCR Primer II A (Takara Bio) and subsequently purified using Ampure XP beads (Beckman). The Illumina library was prepared using Nextera XT DNA library preparation kit (Illumina) and sequenced using an Illumina Novaseq. Raw counts obtained by mRNA sequencing were Rfiltered (genes with counts≥34), normalized and differentially analyzed (|FC|≥ 2 and FDR-adjusted P-value≤0.05) using DEq2 v1.36.0 (Love et al., 2014). Reads were aligned to the mouse genome version mm39. PCA plot and volcano plots were generated using ggplot2 v3.3.5 (Wickham, 2016) and ggrepel v0.9.1 (https://ggrepel.slowkow.com). Ingenuity Pathway Analysis v.90348151 (Qiagen; https://digitalinsights.qiagen.com/IPA) was used to identify likely upstream transcriptional regulators that were linked to the DEG datasets based on changes in expression. We used Benjamini-Hochberg adjusted P-value<0.01 as the significance threshold. For analysis of TEs, TEs were quantified and annotated using TEtranscripts v2.2.3 (Jin et al., 2015). TE counts were filtered, normalized and processed using DESeq2 v1.36.0 (Love et al., 2014) in a similar way as RNA-seq analysis. Bar plots of the proportion of TE reads were generated using GraphPad Prism 9. Only TE classes that contributed a minimum of 1% of the total reads were presented. For analysis of ZGA genes, genes belonging to different ZGA categories (major, minor, and major and minor) were annotated using datasets identified in Abe et al. (2018). Bar plots were generated using ggplot2 v3.3.5 (Wickham, 2016). Upstream regulator analysis of significant differentially expressed ZGA genes was carried out with Ingenuity Pathway Analysis and clusters further annotated using PANTHER GO enrichment analysis (http://geneontology.org/).

Statistical analysis

All experiments were performed with a minimum of three independent replicates, with sample sizes indicated in the text or figure legends. Statistical analysis was performed using GraphPad Prism 9. Fertility data, immunofluorescence quantification and RT-qPCR analyses are displayed as the mean and standard error of the mean (s.e.m.). Unpaired Student's t-test was used to determine the difference between two groups. ELISA data were log-transformed prior to statistical analysis using unpaired Student's t-test or Welch's t-test as indicated. All t-tests were two-tailed. Chromosome alignment, chromosome configuration and transcriptional activity were analyzed using Fisher's exact test on raw data. P<0.05 was considered to be statistically significant.

Acknowledgements

The authors would like to thank the directors and staff at the following advanced technology core facilities at Baylor College of Medicine: Human Tissue Acquisition and Pathology Core, Optical Imaging and Vital Microscopy Core, and Dr Rui Chen and the Single Cell Genomics Core. Core facilities at Baylor College of Medicine are supported by a CPRIT Core Facility Support Award (CPRIT-RP180672) and the NIH (P30 CA125123). We additionally thank Dr Diana Monsivais and Bethany Patton (Baylor College of Medicine) for helpful discussions and comments, and Dr Cecilia Blengini (Rutgers University) for assistance with chromosome spreads. We thank additional members of the Pangas, Monsivais and Hartig laboratories for helpful discussions.

Competing interests

The authors declare no competing or financial interests.

Author contributions

Conceptualization: S.M.B., S.A.P.; Methodology: S.M.B., A.A.A., P.J., K.S.; Formal analysis: T.E.S., P.J., S.A.P.; Investigation: S.M.B.; Resources: S.M.H.; Writing - original draft: S.M.B., S.A.P.; Writing - review & editing: S.M.B., T.E.S., K.S.; Visualization: T.E.S.; Supervision: K.S., S.A.P.; Project administration: S.A.P.; Funding acquisition: S.A.P.

Funding

Support for these studies was provided by the National Institutes of Health grants R01HD085994, R21HD109807, T32HD098068 (to S.A.P.), DK114356 (to S.M.H.) and R35GM136340 (to K.S.). S.M.B. and A.A.A. were supported by pre-doctoral fellowships from T32HD098068. Deposited in PMC for release after 12 months.

Data availability

RNA-sequencing data have been deposited in Gene Expression Omnibus under the accession number GSE218484. All other relevant data can be found within the article and its supplementary information.

Peer review history

The peer review history is available online at https://journals.biologists.com/dev/lookup/doi/10.1242/dev.201535.reviewer-comments.pdf

References

Abbas, T. (2021). The role of ubiquitination and SUMOylation in DNA replication. *Curr. Issues Mol. Biol.* **40**, 189-220. doi:10.21775/cimb.040.189

Abe, K.-I., Funaya, S., Tsukioka, D., Kawamura, M., Suzuki, Y., Suzuki, M. G., Schultz, R. M. and Aoki, F. (2018). Minor zygotic gene activation is essential for mouse preimplantation development. *Proc. Natl. Acad. Sci. USA* **115**, E6780-E6788. doi:10.1073/pnas.1804309115

Albertini, D. F. (2002). The structural basis of oocyte-granulosa cell communication. *Ernst Schering Res. Found. Workshop* **41**, 101-110. doi:10.1007/978-3-662-04960-0_7

Aoki, F. (2022). Zygotic gene activation in mice: profile and regulation. *J. Reprod. Dev.* **68**, 79-84. doi:10.1262/jrd.2021-129

Bhagwat, N. R., Owens, S. N., Ito, M., Boinapalli, J. V., Poa, P., Ditzel, A., Kopparapu, S., Mahalawat, M., Davies, O. R., Collins, S. R. et al. (2021). SUMO is a pervasive regulator of meiosis. *eLife* **10**, e57720. doi:10.7554/eLife.57720

Bouniol-Baly, C., Hamraoui, L., Guibert, J., Beaujean, N., Szöllösi, M. S. and Debey, P. (1999). Differential transcriptional activity associated with chromatin configuration in fully grown mouse germinal vesicle oocytes. *Biol. Reprod.* **60**, 580-587. doi:10.1095/biolreprod60.3.580

Buccione, R., Schroeder, A. C. and Eppig, J. J. (1990). Interactions between somatic cells and germ cells throughout mammalian oogenesis. *Biol. Reprod.* **43**, 543-547. doi:10.1095/biolreprod43.4.543

Bullejos, M. and Koopman, P. (2004). Germ cells enter meiosis in a rostro-caudal wave during development of the mouse ovary. *Mol. Reprod. Dev.* **68**, 422-428. doi:10.1002/mrd.20105

Burns, K. H., Viveiros, M. M., Ren, Y., Wang, P., Demayo, F. J., Frail, D. E., Eppig, J. J. and Matzuk, M. M. (2003). Roles of NPM2 in chromatin and nucleolar organization in oocytes and embryos. *Science* **300**, 633-636. doi:10.1126/science.1081813

Chousal, J. N., Cho, K., Ramaiah, M., Skarbrevik, D., Mora-Castilla, S., Stumpo, D. J., Lykke-Andersen, J., Laurent, L. C., Blackshear, P. J., Wilkinson, M. F. et al. (2018). Chromatin modification and global transcriptional silencing in the oocyte mediated by the mRNA decay activator ZFP36L2. *Dev. Cell* **44**, 392-402.e7. doi:10.1016/j.devcel.2018.01.006

Choy, J. S., Acuña, R., Au, W.-C. and Basrai, M. A. (2011). A role for histone H4K16 hypoacetylation in Saccharomyces cerevisiae kinetochore function. *Genetics* **189**, 11-21. doi:10.1534/genetics.111.130781

Cossec, J.-C., Theurillat, I., Chica, C., Búa Aguín, S., Gaume, X., Andrieux, A., Iturbide, A., Jouvion, G., Li, H., Bossis, G. et al. (2018). SUMO safeguards

somatic and pluripotent cell identities by enforcing distinct chromatin states. *Cell Stem Cell* **23**, 742-757.e8. doi:10.1016/j.stem.2018.10.001

Cox, A. R., Chernis, N., Kim, K. H., Masschelin, P. M., Saha, P. K., Briley, S. M., Sharp, R., Li, X., Felix, J. B., Sun, Z. et al. (2021). Ube2i deletion in adipocytes causes lipoatrophy in mice. *Mol. Metab.* **48**, 101221. doi:10.1016/j.molmet.2021.101221

Dahl, J. A., Jung, I., Aanes, H., Greggains, G. D., Manaf, A., Lerdrup, M., Li, G., Kuan, S., Li, B., Lee, A. Y. et al. (2016). Broad histone H3K4me3 domains in mouse oocytes modulate maternal-to-zygotic transition. *Nature* **537**, 548-552. doi:10.1038/nature19360

De Iaco, A., Planet, E., Coluccio, A., Verp, S., Duc, J. and Trono, D. (2017). DUX-family transcription factors regulate zygotic genome activation in placental mammals. *Nat. Genet.* **49**, 941-945. doi:10.1038/ng.3858

De La Fuente, R. and Eppig, J. J. (2001). Transcriptional activity of the mouse oocyte genome: companion granulosa cells modulate transcription and chromatin remodeling. *Dev. Biol.* **229**, 224-236. doi:10.1006/dbio.2000.9947

De La Fuente, R., Viveiros, M. M., Burns, K. H., Adashi, E. Y., Matzuk, M. M. and Eppig, J. J. (2004). Major chromatin remodeling in the germinal vesicle (GV) of mammalian oocytes is dispensable for global transcriptional silencing but required for centromeric heterochromatin function. *Dev. Biol.* **275**, 447-458. doi:10.1016/j.ydbio.2004.08.028

De Vries, W. N., Binns, L. T., Fancher, K. S., Dean, J., Moore, R., Kemler, R. and Knowles, B. B. (2000). Expression of Cre recombinase in mouse oocytes: a means to study maternal effect genes. *Genesis* **26**, 110-112. doi:10.1002/(SICI)1526-968X(200002)26:2<110::AID-GENE2>3.0.CO;2-8

Debey, P., Szöllösi, M. S., Szöllösi, D., Vautier, D., Girousse, A. and Besombes, D. (1993). Competent mouse oocytes isolated from antral follicles exhibit different chromatin organization and follow different maturation dynamics. *Mol. Reprod. Dev.* **36**, 59-74. doi:10.1002/mrd.1080360110

Durlinger, A. L. L., Kramer, P., Karels, B., de Jong, F. H., Uilenbroek, J. T. J., Grootegoed, J. A. and Themmen, A. P. N. (1999). Control of primordial follicle recruitment by anti-Mullerian hormone in the mouse ovary. *Endocrinology* **140**, 5789-5796. doi:10.1210/endo.140.12.7204

Durlinger, A. L., Visser, J. A. and Themmen, A. P. (2002). Regulation of ovarian function: the role of anti-Mullerian hormone. *Reproduction* **124**, 601-609. doi:10.1530/rep.0.1240601

El Yakoubi, W., Buffin, E., Cladière, D., Gryaznova, Y., Berenguer, I., Touati, S. A., Gómez, R., Suja, J. A., van Deursen, J. M. and Wassmann, K. (2017). Mps1 kinase-dependent Sgo2 centromere localisation mediates cohesin protection in mouse oocyte meiosis I. *Nat. Commun.* **8**, 694. doi:10.1038/s41467-017-00774-3

Evsikov, A. V., De Vries, W. N., Peaston, A. E., Radford, E. E., Fancher, K. S., Chen, F. H., Blake, J. A., Bult, C. J., Latham, K. E., Solter, D. et al. (2004). Systems biology of the 2-cell mouse embryo. *Cytogenet Genome Res.* **105**, 240-250. doi:10.1159/000078195

Feitosa, W. B. and Morris, P. L. (2018). SUMOylation regulates germinal vesicle breakdown and the Akt/PKB pathway during mouse oocyte maturation. *Am. J. Physiol. Cell Physiol.* **315**, C115-C121. doi:10.1152/ajpcell.00038.2018

Feitosa, W. B., Hwang, K. S. and Morris, P. L. (2018). Temporal and SUMO-specific SUMOylation contribute to the dynamics of Polo-like kinase 1 (PLK1) and spindle integrity during mouse oocyte meiosis. *Dev. Biol.* **434**, 278-291. doi:10.1016/j.ydbio.2017.12.011

Fortune, J. E. (2002). Activation of primordial follicles. *Ernst Schering Res. Found. Workshop* **41**, 11-21. doi:10.1007/978-3-662-04960-0_2

Garvin, A. J. (2019). Beyond reversal: ubiquitin and ubiquitin-like proteases and the orchestration of the DNA double strand break repair response. *Biochem. Soc. Trans.* **47**, 1881-1893. doi:10.1042/BST20190534

Hanna, C. W., Demond, H. and Kelsey, G. (2018). Epigenetic regulation in development: is the mouse a good model for the human? *Hum. Reprod. Update* **24**, 556-576. doi:10.1093/humupd/dmy021

Hendrickson, P. G., Doráis, J. A., Grow, E. J., Whiddon, J. L., Lim, J.-W., Wike, C. L., Weaver, B. D., Pflueger, C., Emery, B. R., Wilcox, A. L. et al. (2017). Conserved roles of mouse DUX and human DUX4 in activating cleavage-stage genes and MERVL/HERVL retrotransposons. *Nat. Genet.* **49**, 925-934. doi:10.1038/ng.3844

Higuchi, C., Yamamoto, M., Shin, S.-W., Miyamoto, K. and Matsumoto, K. (2019). Perturbation of maternal PIASy abundance disrupts zygotic genome activation and embryonic development via SUMOylation pathway. *Biol. Open* **8**, bio048652. doi:10.1242/bio.048652

Hirshfield, A. N. and Midgley, A. R.Jr. (1978). Morphometric analysis of follicular development in the rat. *Biol. Reprod.* **19**, 597-605. doi:10.1095/biolreprod19.3.597

Jin, Y., Tam, O. H., Paniagua, E. and Hammell, M. (2015). TEtranscripts: a package for including transposable elements in differential expression analysis of RNA-seq datasets. *Bioinformatics* **31**, 3593-3599. doi:10.1093/bioinformatics/btv422

Kageyama, S.-I., Liu, H., Kaneko, N., Ooga, M., Nagata, M. and Aoki, F. (2007). Alterations in epigenetic modifications during oocyte growth in mice. *Reproduction* **133**, 85-94. doi:10.1530/REP-06-0025

Kigami, D., Minami, N., Takayama, H. and Imai, H. (2003). MuERV-L is one of the earliest transcribed genes in mouse one-cell embryos. *Biol. Reprod.* **68**, 651-654. doi:10.1095/biolreprod.102.007906

Kramer, A., Green, J., Pollard, J., Jr. and Tugendreich, S. (2014). Causal analysis approaches in Ingenuity Pathway Analysis. *Bioinformatics* **30**, 523-530. doi:10.1093/bioinformatics/btt703

Lan, Z.-J., Xu, X. and Cooney, A. J. (2004). Differential oocyte-specific expression of Cre recombinase activity in GDF-9-iCre, Zp3cre, and Msx2Cre transgenic mice. *Biol. Reprod.* **71**, 1469-1474. doi:10.1095/biolreprod.104.031757

Lee, M. T., Bonneau, A. R. and Giraldez, A. J. (2014). Zygotic genome activation during the maternal-to-zygotic transition. *Annu. Rev. Cell Dev. Biol.* **30**, 581-613. doi:10.1146/annurev-cellbio-100913-013027

Livak, K. J. and Schmittgen, T. D. (2001). Analysis of relative gene expression data using real-time quantitative PCR and the 2(−Delta Delta C(T)) Method. *Methods* **25**, 402-408. doi:10.1006/meth.2001.1262

Love, M. I., Huber, W. and Anders, S. (2014). Moderated estimation of fold change and dispersion for RNA-seq data with DESeq2. *Genome Biol.* **15**, 550. doi:10.1186/s13059-014-0550-8

Low, Y., Tan, D. E. K., Hu, Z., Tan, S. Y. X. and Tee, W.-W. (2021). Transposable element dynamics and regulation during zygotic genome activation in mammalian embryos and embryonic stem cell model systems. *Stem Cells Int.* **2021**, 1624669. doi:10.1155/2021/1624669

Ma, P. and Schultz, R. M. (2013). Histone deacetylase 2 (HDAC2) regulates chromosome segregation and kinetochore function via H4K16 deacetylation during oocyte maturation in mouse. *PLoS Genet.* **9**, e1003377. doi:10.1371/journal.pgen.1003377

Ma, J.-Y., Li, M., Luo, Y.-B., Song, S., Tian, D., Yang, J., Zhang, B., Hou, Y., Schatten, H., Liu, Z. et al. (2013). Maternal factors required for oocyte developmental competence in mice: transcriptome analysis of non-surrounded nucleolus (NSN) and surrounded nucleolus (SN) oocytes. *Cell Cycle* **12**, 1928-1938. doi:10.4161/cc.24991

Mattson, B. A. and Albertini, D. F. (1990). Oogenesis: chromatin and microtubule dynamics during meiotic prophase. *Mol. Reprod. Dev.* **25**, 374-383. doi:10.1002/mrd.1080250411

Medvedev, S., Pan, H. and Schultz, R. M. (2011). Absence of MSY2 in mouse oocytes perturbs oocyte growth and maturation, RNA stability, and the transcriptome. *Biol. Reprod.* **85**, 575-583. doi:10.1095/biolreprod.111.091710

Miyara, F., Migne, C., Dumont-Hassan, M., Le Meur, A., Cohen-Bacrie, P., Aubriot, F.-X., Glissant, A., Nathan, C., Douard, S., Stanovici, A. et al. (2003). Chromatin configuration and transcriptional control in human and mouse oocytes. *Mol. Reprod. Dev.* **64**, 458-470. doi:10.1002/mrd.10233

Mizunuma, H., Liu, X., Andoh, K., Abe, Y., Kobayashi, J., Yamada, K., Yokota, H., Ibuki, Y. and Hasegawa, Y. (1999). Activin from secondary follicles causes small preantral follicles to remain dormant at the resting stage. *Endocrinology* **140**, 37-42. doi:10.1210/endo.140.1.6409

Monti, M., Zanoni, M., Calligaro, A., Ko, M. S. H., Mauri, P. and Redi, C. A. (2013). Developmental arrest and mouse antral not-surrounded nucleolus oocytes. *Biol. Reprod.* **88**, 2. doi:10.1095/biolreprod.112.103887

Nacerddine, K., Lehembre, F., Bhaumik, M., Artus, J., Cohen-Tannoudji, M., Babinet, C., Pandolfi, P. P. and Dejean, A. (2005). The SUMO pathway is essential for nuclear integrity and chromosome segregation in mice. *Dev. Cell* **9**, 769-779. doi:10.1016/j.devcel.2005.10.007

Neyret-Kahn, H., Benhamed, M., Ye, T., Le Gras, S., Cossec, J.-C., Lapaquette, P., Bischof, O., Ouspenskaia, M., Dasso, M., Seeler, J. et al. (2013). Sumoylation at chromatin governs coordinated repression of a transcriptional program essential for cell growth and proliferation. *Genome Res.* **23**, 1563-1579. doi:10.1101/gr.154872.113

Nguyen, A. L., Drutovic, D., Vazquez, B. N., El Yakoubi, W., Gentilello, A. S., Malumbres, M., Solc, P. and Schindler, K. (2018). Genetic interactions between the aurora kinases reveal new requirements for AURKB and AURKC during oocyte meiosis. *Curr. Biol.* **28**, 3458-3468.e5. doi:10.1016/j.cub.2018.08.052

Nottke, A. C., Kim, H.-M. and Colaiácovo, M. P. (2017). Wrestling with chromosomes: the roles of SUMO during meiosis. *Adv. Exp. Med. Biol.* **963**, 185-196. doi:10.1007/978-3-319-50044-7_11

Ouyang, J. and Gill, G. (2009). SUMO engages multiple corepressors to regulate chromatin structure and transcription. *Epigenetics* **4**, 440-444. doi:10.4161/epi.4.7.9807

Pangas, S. A. (2012). Regulation of the ovarian reserve by members of the transforming growth factor beta family. *Mol. Reprod. Dev.* **79**, 666-679. doi:10.1002/mrd.22076

Pangas, S. A., Li, X., Robertson, E. J. and Matzuk, M. M. (2006). Premature luteinization and cumulus cell defects in ovarian-specific Smad4 knockout mice. *Mol. Endocrinol.* **20**, 1406-1422. doi:10.1210/me.2005-0462

Pangas, S. A., Li, X., Umans, L., Zwijsen, A., Huylebroeck, D., Gutierrez, C., Wang, D., Martin, J. F., Jamin, S. P., Behringer, R. R. et al. (2008). Conditional deletion of Smad1 and Smad5 in somatic cells of male and female gonads leads to metastatic tumor development in mice. *Mol. Cell. Biol.* **28**, 248-257. doi:10.1128/MCB.01404-07

Pedersen, T. and Peters, H. (1968). Proposal for a classification of oocytes and follicles in the mouse ovary. *J. Reprod. Fertil.* **17**, 555-557. doi:10.1530/jrf.0.0170555

Peng, J., Li, Q., Wigglesworth, K., Rangarajan, A., Kattamuri, C., Peterson, R. T., Eppig, J. J., Thompson, T. B. and Matzuk, M. M. (2013). Growth differentiation factor 9:bone morphogenetic protein 15 heterodimers are potent regulators of ovarian functions. *Proc. Natl. Acad. Sci. USA* **110**, E776-E785. doi:10.1073/pnas.1218020110

Ploutarchou, P., Melo, P., Day, A. J., Milner, C. M. and Williams, S. A. (2015). Molecular analysis of the cumulus matrix: insights from mice with O-glycan-deficient oocytes. *Reproduction* **149**, 533-543. doi:10.1530/REP-14-0503

Richard, P., Vethantham, V. and Manley, J. L. (2017). Roles of sumoylation in mRNA processing and metabolism. *Adv. Exp. Med. Biol.* **963**, 15-33. doi:10.1007/978-3-319-50044-7_2

Rodriguez, A., Briley, S. M., Patton, B. K., Tripurani, S. K., Rajapakshe, K., Coarfa, C., Rajkovic, A., Andrieux, A., Dejean, A. and Pangas, S. A. (2019). Loss of the E2 SUMO-conjugating enzyme Ube2i in oocytes during ovarian folliculogenesis causes infertility in mice. *Development* **146**, dev176701. doi:10.1242/dev.176701

Ruta, V., Pagliarini, V. and Sette, C. (2021). Coordination of RNA processing regulation by signal transduction pathways. *Biomolecules* **11**, 1475. doi:10.3390/biom11101475

Schellander, K., Hoelker, M. and Tesfaye, D. (2007). Selective degradation of transcripts in mammalian oocytes and embryos. *Theriogenology* **68** Suppl. 1, S107-S115. doi:10.1016/j.theriogenology.2007.05.054

Schindler, K. (2011). Protein kinases and protein phosphatases that regulate meiotic maturation in mouse oocytes. *Results Probl. Cell Differ.* **53**, 309-341. doi:10.1007/978-3-642-19065-0_14

Schultz, R. M., Stein, P. and Svoboda, P. (2018). The oocyte-to-embryo transition in mouse: past, present, and future. *Biol. Reprod.* **99**, 160-174. doi:10.1093/biolre/ioy013

Sherman, B. T., Hao, M., Qiu, J., Jiao, X., Baseler, M. W., Lane, H. C., Imamichi, T. and Chang, W. (2022). DAVID: a web server for functional enrichment analysis and functional annotation of gene lists (2021 update). *Nucleic Acids Res.* **50**, W216-W221. doi:10.1093/nar/gkac194

Smith, R., Susor, A., Ming, H., Tait, J., Conti, M., Jiang, Z. and Lin, C.-J. (2022). The H3.3 chaperone Hira complex orchestrates oocyte developmental competence. *Development* **149**, dev200044. doi:10.1242/dev.200044

Su, Y.-Q., Wu, X., O'Brien, M. J., Pendola, F. L., Denegre, J. N., Matzuk, M. M. and Eppig, J. J. (2004). Synergistic roles of BMP15 and GDF9 in the development and function of the oocyte-cumulus cell complex in mice: genetic evidence for an oocyte-granulosa cell regulatory loop. *Dev. Biol.* **276**, 64-73. doi:10.1016/j.ydbio.2004.08.020

Su, Y.-Q., Sugiura, K., Woo, Y., Wigglesworth, K., Kamdar, S., Affourtit, J. and Eppig, J. J. (2007). Selective degradation of transcripts during meiotic maturation of mouse oocytes. *Dev. Biol.* **302**, 104-117. doi:10.1016/j.ydbio.2006.09.008

Theurillat, I., Hendriks, I. A., Cossec, J.-C., Andrieux, A., Nielsen, M. L. and Dejean, A. (2020). Extensive SUMO modification of repressive chromatin factors distinguishes pluripotent from somatic cells. *Cell Rep.* **32**, 108146. doi:10.1016/j.celrep.2020.108146

Tilly, J. L. (2003). Ovarian follicle counts–not as simple as 1, 2, 3. *Reprod. Biol. Endocrinol.* **1**, 11. doi:10.1186/1477-7827-1-11

Tong, Z.-B., Gold, L., Pfeifer, K. E., Dorward, H., Lee, E., Bondy, C. A., Dean, J. and Nelson, L. M. (2000). Mater, a maternal effect gene required for early embryonic development in mice. *Nat. Genet.* **26**, 267-268. doi:10.1038/81547

Tripathi, A., Kumar, K. V. P. and Chaube, S. K. (2010). Meiotic cell cycle arrest in mammalian oocytes. *J. Cell. Physiol.* **223**, 592-600. doi:10.1002/jcp.22108

Vertegaal, A. C. O. (2022). Signalling mechanisms and cellular functions of SUMO. *Nat. Rev. Mol. Cell Biol.* **23**, 715-731. doi:10.1038/s41580-022-00500-y

Walser, C. B. and Lipshitz, H. D. (2011). Transcript clearance during the maternal-to-zygotic transition. *Curr. Opin. Genet. Dev.* **21**, 431-443. doi:10.1016/j.gde.2011.03.003

Wickham, H. (2016). *Elegant Graphics for Data Analysis*. New York: Springer-Verlag.

Wigglesworth, K., Lee, K.-B., O'Brien, M. J., Peng, J., Matzuk, M. M. and Eppig, J. J. (2013). Bidirectional communication between oocytes and ovarian follicular somatic cells is required for meiotic arrest of mammalian oocytes. *Proc. Natl. Acad. Sci. USA* **110**, E3723-E3729. doi:10.1073/pnas.1314829110

Wu, X., Viveiros, M. M., Eppig, J. J., Bai, Y., Fitzpatrick, S. L. and Matzuk, M. M. (2003). Zygote arrest 1 (Zar1) is a novel maternal-effect gene critical for the oocyte-to-embryo transition. *Nat. Genet.* **33**, 187-191. doi:10.1038/ng1079

Yuan, Y.-F., Zhai, R., Liu, X.-M., Khan, H. A., Zhen, Y.-H. and Huo, L.-J. (2014). SUMO-1 plays crucial roles for spindle organization, chromosome congression, and chromosome segregation during mouse oocyte meiotic maturation. *Mol. Reprod. Dev.* **81**, 712-724. doi:10.1002/mrd.22339

Zeng, F. and Schultz, R. M. (2005). RNA transcript profiling during zygotic gene activation in the preimplantation mouse embryo. *Dev. Biol.* **283**, 40-57. doi:10.1016/j.ydbio.2005.03.038

Zhang, B., Zheng, H., Huang, B., Li, W., Xiang, Y., Peng, X., Ming, J., Wu, X., Zhang, Y., Xu, Q. et al. (2016). Allelic reprogramming of the histone modification H3K4me3 in early mammalian development. *Nature* **537**, 553-557. doi:10.1038/nature19361

Zhu, J.-L., Lin, S.-L., Li, M., Ouyang, Y.-C., Hou, Y., Schatten, H. and Sun, Q.-Y. (2010). Septin2 is modified by SUMOylation and required for chromosome congression in mouse oocytes. *Cell Cycle* **9**, 1607-1616. doi:10.4161/cc.9.8.11463

Zuccotti, M., Piccinelli, A., Giorgi Rossi, P., Garagna, S. and Redi, C. A. (1995). Chromatin organization during mouse oocyte growth. *Mol. Reprod. Dev.* **41**, 479-485. doi:10.1002/mrd.1080410410

Zuccotti, M., Giorgi Rossi, P., Martinez, A., Garagna, S., Forabosco, A. and Redi, C. A. (1998). Meiotic and developmental competence of mouse antral oocytes. *Biol. Reprod.* **58**, 700-704. doi:10.1095/biolreprod58.3.700